REPORTS IN METEOROLOGY AND OCEANOGRAPHY
UNIVERSITY OF BERGEN 1 - 2008

# Hydro- and thermodynamics related to CO2-fluxes through the sea floor

By

Sönke Maus

UNIVERSITY OF BERGEN

Geophysical Institute
Allegaten 70
5007 Bergen
Norway

**«REPORTS IN METEOROLOGY AND OCEANOGRAPHY»**
**utgis av Geofysisk Institutt ved Universitetet I Bergen.**
**Formålet med rapportserien er å publisere arbeider av personer som er tilknyttet avdelingen.**
**Redaksjonsutvalg:**
**Peter M. Haugan, Frank Cleveland, Arvid Skartveit og Endre Skaar.**
**Redaksjonens adresse er : «Reports in Meteorology and Oceanography», Geophysical Institute.**
**Allégaten 70**
**N-5007 Bergen, Norway**

**RAPPORT NR: 1 - 2008**
**ISSN 1502-5519**
**ISBN 82-8116-013-6**

# Preface

The CLIMIT programme under the Norwegian Research Council, awarded a contract to the University of Bergen in April 2007 for a review study on possible marine impacts from storing CO2 under the seabed. The work has been conducted by the following partners: Christian Michelsen Research (CMR), NIVA, Geophysical Institute (GFI, UiB), Department of Mathematics (MI, UiB), and Bergen Center for Computational Science (BCCS, Unifob).

The study "**Geological storage of CO2 - The marine component"** was divided into four work packages with the following tasks:
• WP 1: Project coordination, including arranging a workshop (BCCS)
• WP 2: Impact on sediments, seawater and marine biota (NIVA)
• WP 3: The benthic boundary layer dynamics (UiB, GFI)
• WP 4: Monitoring and detection of seeps and CO2 in seawater (CMR)

The results from the work packages 1, 2 and 4 can be found as:
• WR 1: Presentations from a workshop: http://www.cmu.uib.no/subseastorage
• WP 2: NIVA report nr. 5478-2007 "Sub-seabed storage of CO2. Impact on sediments, seawater and marine biota from leaks"
• WP 4: "Monitoring and detection of seeps and CO2 in seawater" as report CMR-07-F10808-RA-1.

The present report is the contribution WP 3 by the Geophysical Institute (GFI, UiB). The latter was originally planned as a review of oceanic bottom boundary dynamics. Due to the manifold in ongoing research on physical problems related to the leakage of CO2, including the thermodynamics of pure CO2 and mixed seawater-CO2 systems, droplet plume dynamics, ocean-seabed interaction, as well as stability and permeability aspects of the seabed itself, the original topic has been extended. The title of the present report **"Hydro- and thermodynamics related to CO2-fluxes through the seafloor"** reflects this extension.

Bergen, January 2008

Sönke Maus

Geological storage of $CO_2$
The marine component

CLIMIT Report

# Hydro- and thermodynamics related to $CO_2$-fluxes near the sea floor

by Sönke Maus

Geophysical Institute, University of Bergen
Allegaten 70, 5007 Bergen, Norway

Bergen, January 2008

# Contents

# 1 Background: $CO_2$ storage

The past decades have resulted in the consent among scientists that the release of greenhouse gases by human beings has begun to change climate on earth - and will increasingly do so in the future (IPCC, 2007a). More than 60 % of the anthropogenic greenhouse effect is related to carbondioxide release due to burning of fossil fuels. Actual global emmissions of $C0_2$ imply, both due to the increasing energy usage in developing countries, and the continuous increase in industrial countries, a rise in atmospheric $C0_2$ that even exceeds the worst scenarios from the IPCC (Figure 1). The severity of the problem may be envisaged by quoting the lifetime of anthropogenic atmospheric $C0_2$ in the biosphere in the popular form suggested by Archer (2005): *300 years, plus 25 % that lasts forever.*

## 1.1 Climate change mitigation

To avoid the serious risks of rapid climate change it is necessary to prosecute actively all available mitigation options. The sustainable longterm goal, a stabilisation of atmospheric $C0_2$ concentration by energy saving and renewable production, requires severe transformations of the present global energy infrastructure and societies (Parson and Keith, 1998). A realistic evaluation of the present global situation points to the likelihood, that the expectable transformation will be too slow to mitigate climate change problems, if not methods of geoengineering are considered. One of the first suggested geoengineering approaches was injection and dissolution of liquid $C0_2$ in the ocean (Marchetti, 1977). Recently also the possibility to influence the radiation balance of the upper atmosphere has been considered (MacCracken, 2006). The at present, in terms of technology, safety and scientific clarity, most realistic approaches of climate change mitigation by geoengineering appear to be related to the field of carbon capture and storage (CCS) (IPCC, 2007b). These employ carbon capture in an oil-, gas- or coal-fired power plant, followed by (i) mineral carbonation, (ii) direct injection into the ocean or (iii) storage in geological formations, terrestrial and below the ocean floor (Figure 3). Assessment models of climate change mitigation indicate that CCS is capable to provide a fraction of 20 to 30 % of global emission reductions during the next century (Figure 2).

## 1.2 Carbon capture and storage (CCS)

The present scientific state of the art on Carbone Capture and Storage (CCS) has been summarised by the Intergovernmental Panel of Climate Change IPCC (2007b) and others (Göttlicher, 2006; Fischedick et al., 2007). On the one hand, $\approx 85\%$ of $CO_2$ emitted from a power plant may be captured by modern techniques. On the other hand, capture implies an increase in the energy requirement by 15 to 30 %, and an increase in the capital costs for energy production by 40 to 80 %. For transport and storage another cost penalty of each $5-15$ % has to be added, which raises the overall cost penalty of CCS to 50 to 110 %. As costs are, in the present world, intimately related to energy consumption, one expects

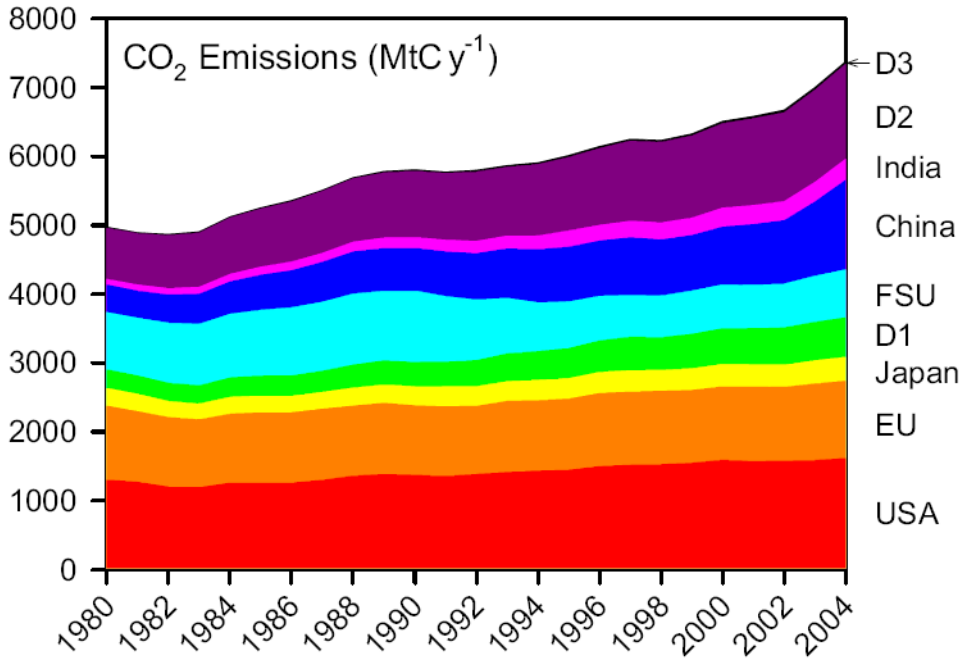


Figure 1: Evolution of $C0_2$ emissions for different groups of countries. From Raupach et al. (2007).

that CCS will increase the brutto emission of $CO_2$ by $20-40$ %. In connection with the capturing potential of $\approx 85$ % this means that effective $CO_2$ emissions may be reduced to $\approx 20$ % of the values without CCS. This potential may apply to $\approx 60$ % of the present fossil fuel burn, excluding emissions from dispersed sources like buildings and vehicles, and it thus leads to the reduction potential indicated in Figure 2.

Due to the $\approx 20-40$ % increase in energy consumption it is clear that the storage of CCS must be safe and sustainable. Otherwise it will increase the problems that it aims to solve. In this sense one must distinguish between time scales of oceanic and geological storage, to be outlined below.

### 1.2.1 Sequestration in the ocean: Dissolution is no solution

The possibility of $CO_2$ sequestration by direct injection into the ocean was first considered by Marchetti (1977). The present state-of-the-art simulations indicate that, in case of shallow injection between 800 and 1500m ocean depth, most of the $CO_2$ captured in the ocean will return to the atmosphere within a few centuries (IPCC, 2007b). Due to the higher brutto emission of $CO_2$ by capture the ocean storage option thus rather delays and increases the problem to future generations. In case of injection in the deep ocean there is, due to liquid $CO_2$ becoming heavier than seawater, a longer residence of 500-1000 years expected, yet the risk of considerable ecological damage of oceanic benthic life is much higher (IPCC, 2007b; Johnston et al., 1999). In this connection it is notable

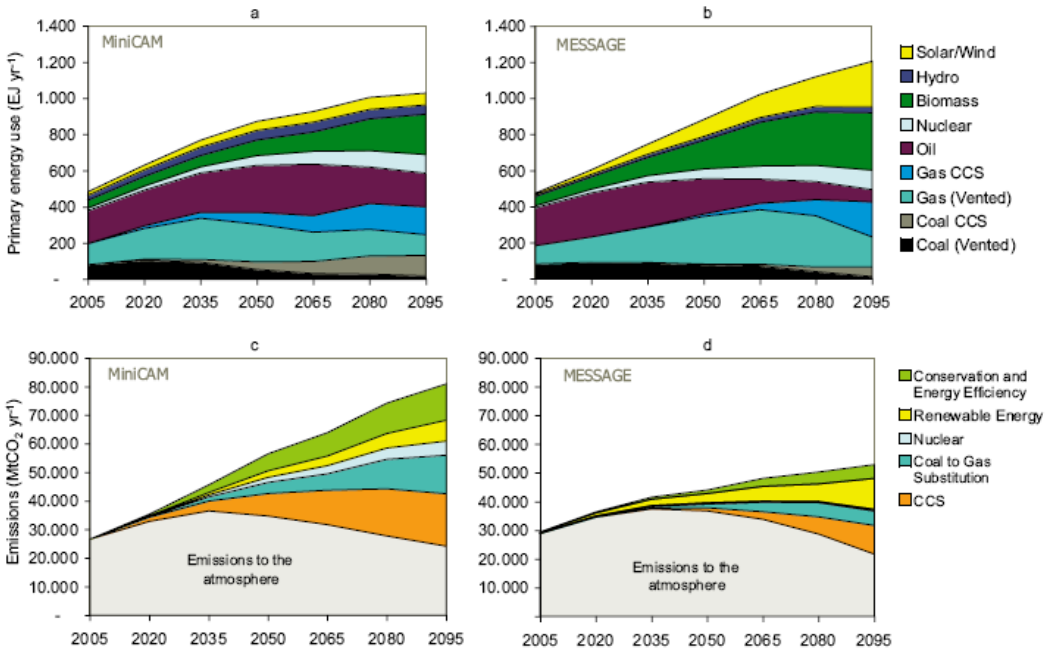


Figure 2: Projections of primary energy use (a and b) due to two assessment models (IPCC, 2007b). The reduction potential of atmospheric emissions indicates the role of CCS in a global mitigation portfolio.

that oceanic pH will already change seriously during the next centuries, due to present and the expectable future emissions to the atmosphere (Figure 4). An enhancement of this signal by direct injection of $CO_2$ into the ocean is likely very problematic (Caldeira and Wickett, 2003; IPCC, 2007b). These aspects make a direct $CO_2$ release into the ocean a rather unsustainable approach to climate change mitigation.

### 1.2.2 Geological storage versus other approaches

The overall storage capacity of $CO_2$ in geological formations is likely 1.5 to 2 $\times 10^3$ $GtCO_2$, with saline formations and oil/gas fields contributing roughly 2/3 and 1/3 and coal seams less than 1% (IPCC, 2007b). Provided that geological storage is save, it is useful to compare these numbers to costs of other mitigation options, and it is important to be aware of the limits of these numbers.

- The world-wide storage capacity of CCS implies that the annual capture in Figure 2 may be realistic for 50 to 150 years beyond the year 2100. This is a large potential, but it clearly points to the bridging character of CCS.

- The costs for capture, transport and storage will most likely be in the range 30 to 70 Euro/$tCO_2$ IPCC (2007b); Fischedick et al. (2007). This compares to an approximately two times larger range of 70 to 150 Euro/$tCO_2$ for capture and re-mineralisation. Notably, emission reductions of 30%

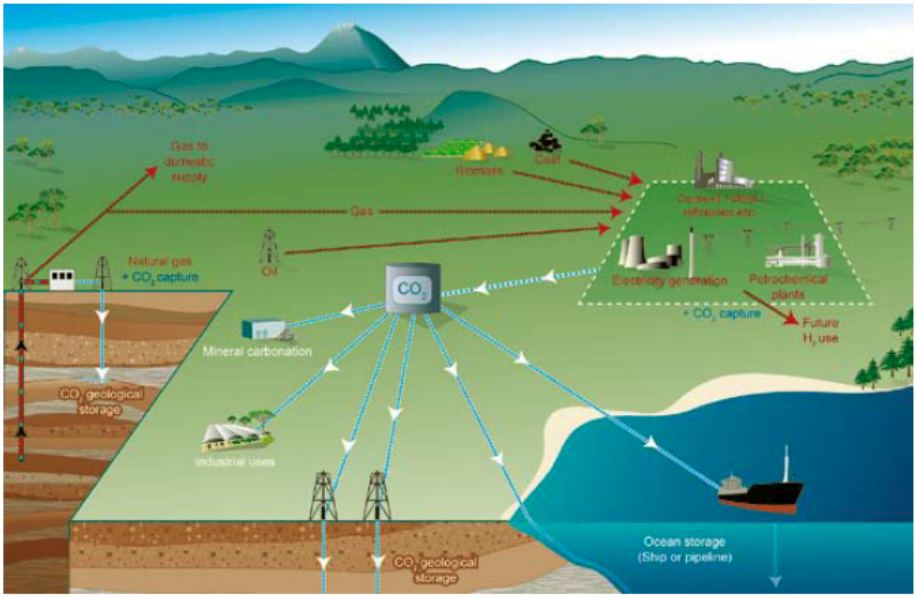


Figure 3: Options of $C0_2$ capture and storage. From IPCC (2007b).

on the basis of intelligent technology and energy efficiency, also included in the scenarios from Figure 2, will cost less than 25 Euro/t$CO_2$, while a certain amount of savings will be available for free. Costs for sequestration by forestation, considering a similar 20-30 % reduction of present emissions, have been estimated as 30-40 Euro/t$CO_2$ (Stavins, 1999).

Hence, there is sufficient storage capacity for CCS to take the role of a bridging function - on the order of a century - as a climate change mitigation option. Costs are comparable to other approaches like, for example, re-forestation. Savings and intelligent renewable energy use must take over in the long-term.

At present the global annual injection into geological reservoirs is around 30 Mt$CO_2$, mostly in west Texas, to recover oil (Enhanced Oil Recovery). Other noteworthy pilot studies are the Weyburn project (Canada), which combines EOR with monitoring, modelling and research, and the annual injection of the order of 1 Mt$CO_2$ in the Sleipner formation (Norway). The climate mitigation target proposed by the IPCC thus requires an increase of the present day storage rates by a factor of 500.

### 1.2.3 Safety of geological storage

The basic mechanisms to be expected for injection of $CO_2$ in (subsea) saline formations are the following (IPCC, 2007b): As liquid $CO_2$ and water are immiscible, the less dense and less viscous liquid $CO_2$ will move upwards in form of plumes. Viscous fingering makes upward movement more easy. When the pore fluid becomes denser by dissolution of $CO_2$, convection cells may form and create a downward transport and effective mixing of $CO_2$ in the formation. Two

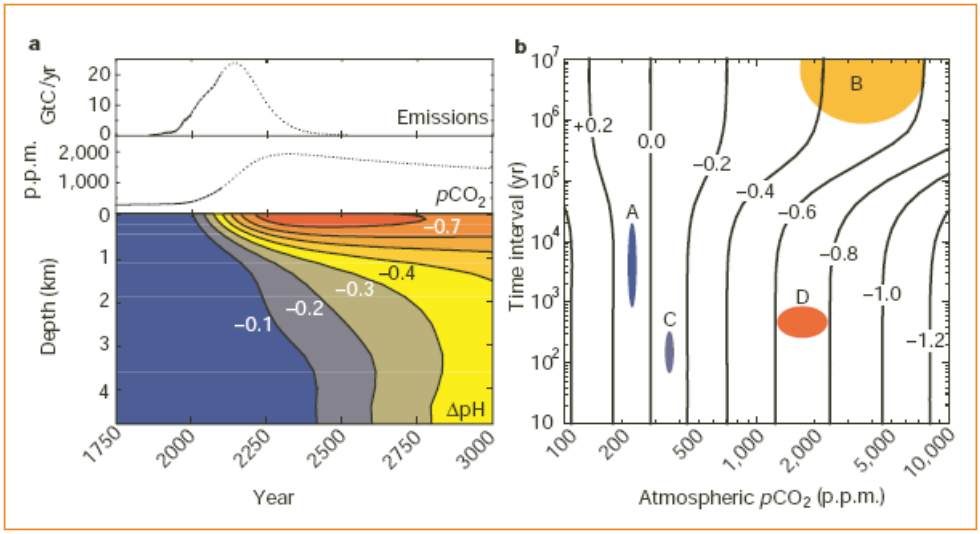


Figure 4: From Caldeira and Wickett (2003): a) Simulated evolution of $CO_2$ emissions, atmospheric $pCO_2$ and oceanic $\Delta$pH compared to its preindustrial value in a probable emission scenario; b) Natural variability and timescales (A,B,C) versus expectable anthropogenic signal (D) in $\Delta$pH.

other processes are expected to be relevant: (i) Some $CO_2$ will also be trapped by capillary forces or dead-ends in the pore space, (ii) $CO_2$ dissolved in water will react with the silicate minerals to form carbonate minerals, thereby chemically trapping the $CO_2$. Adsorption as a third mechanism is relevant in coal seams, yet these contribute only by 1 % to the overall storage capacity, which is mostly due to saline formations.

Convective transport is likely an important trigger for dissolution of $CO_2$ in a saline formation. Simulations of systems with slowly flowing water indicate that during tens of years 30 % of the $CO_2$ will dissolve in the formation fluid, with complete dissolution over centuries. Without fluid flow dissolution is governed by diffusion and local concentration gradients and will take much longer time, $10^2$ to $10^4$ years. Mineralisation is an even slower process for which time scales of $> 10^6$ years can be estimated. Also mineralisation may be enhanced by convection. When saturation levels are reached, convection may lead to outgassing and more complex situations of multiphase flow.

The main aspects of the safety evaluation of geological formations in question for CCS, as evaluated by the IPCC IPCC (2007b) may be summarised as:

- It is considered likely that 99 % of injected $CO_2$ will be retained for 1000 years (at carefully injected sites).

- Trapping below a confining layer (cap-rock) may be enhanced by (i) long-term dissolution in the *in situ* formation fluids, (ii) adsorption onto organic matter in coal and shale, (iii) trapping by reaction with minerals to produce carbonate minerals.

- Potential risks to humans and ecosystems arise from (i) leaking injection wells, (ii) leakage across faults and (iii) ineffective confining layers.

However, there are a number of processes that are not well understood and therefore present uncertainty factors in the evaluation of longterm safety of storage:

- Warming of saturated pore fluid implies degassing of $CO_2$ and possible upward migration of gas bubbles. Such a mechanism may be triggered once convection sets in.

- Reaction of $CO_2$ with rocks and formation water may effect the porosity and permeability of the formation. Observations are not available and modelling studies are sparse. Xu et al. (2003) simulated that precipitation of carbonates may slightly decrease the average porosity and permeability in a reservoir on time scales of 1000-10,000 years. However, such simulations do not account for a possible heterogeneity of reactions and flow. The formation of critical flow paths and localised pore structure changes may, in contrast to homogeneous chemical model predictions, rather enhance the permeability.

- Changes in the chemical, hydrological and mechanical properties may create stresses in the seabed and thus trigger crack formation.

The mentioned unknowns relate to a lack in coupled models of geochemical modelling on the pore-scale and simulations of macroscopic fluid flow. Direct validation of these processes on the field scale is difficult, and the present uncertainty evaluations rely mainly on the comparison of different numerical models (IPCC, 2007b).

### 1.2.4 Sustainability

The term sustainability should be taken literally by recognising that CCS can only overtake a bridging function during the transformation of energy infrastructures and societies towards renewability: This transition time is, due to storage capacities, limited to one to two centuries. Any way of thinking that proposes, due to the possibility of $CO_2$ capture and storage, the continuation of present-day burn of fossil fuels must be questioned. An example of such a way of thinking is the term *negative storage coasts*, introduced by the IPCC in connection with Enhanced Oil Recovery by injection of $CO_2$ (EOR). The latter is considered as an option that avoids $CO_2$ emissions, although the process essentially discharges oil to be converted into $CO_2$ emissions. This logical contradiction clearly points to the necessity to solve future problems by means of rational and ethical, and not simply economical considerations.

## 1.3 Present Report

For a proper evaluation of CCS as a climate change mitigation option model and observational studies are required. These may be grouped into investigations of (i) geological formation safety and (ii) environmental problems that arise when leakage from a storage reservoir occurs. From a geological point of view (i), one has to combine geochemical modelling efforts with monitoring and careful selection of sites for which criteria have been summarised (IPCC, 2007b). According to present day monitoring and modelling one may, if these criteria are followed, expect a retention of more then 99 % of the injected $CO_2$ for 1000 years (IPCC, 2007b). However, these numbers must still be viewed as provisoric and needing more validation studies. While there is considerable work ongoing with respect to more complex simulations and monitoring of geological formation storage, there is a lack in studies of the effects of leakage on the ecosystems near the seafloor (Gale, 2004; IPCC, 2007b).

The present report focuses mainly on the situation that leakage takes place, considering the physical processes that are relevant when a $CO_2$ source is present at the sea floor. It is concerned with hydrodynamic and thermodynamic aspects in the oceanic *Bottom Boundary Layer* (BBL) and in the bottom-near sediments. Investigated topics are (i) thermodynamics of hydrates and their stability, (ii) the hydrodynamics and dissolution of rising droplets, (iii) turbulence and mixing in the oceanic bottom boundary layer, (iv) interaction between sediments, ocean currents and waves. Last but not least, are some stability aspects of porous media, eventually also relevant for seabed fluid flow and seepage through deeper layers, pointed out. Within the frame of the present work it is hardly possible to present a detailed discussion or overview of the mentioned topics. Instead it is focused on specific problems that have been recently addressed in investigations related to $CO_2$ release and storage. It is attempted to review these investigations critically while summarising the main hydrodynamic or thermodynamic background. For more detailed discussions of the physical problems encountered the reader is referred to selected basic textbooks. It is hoped that the present overview helps to get a basic idea of the thermo- and hydrodynamical problems in connection with fluxes near the seafloor. Most of them are not only relevant in terms of climate change mitigation, yet important for a general understanding of the earth's climate system.

# 2 Phase equilibria and thermodynamics of $CO_2$ and seawater

To understand and model two-phase flow and dissolution in mixtures of seawater brine and $CO_2$ one must know the phase equilibria and PVTx-properties for the separated and combined systems. For seawater these are well established in the relevant pressure and temperature range (Fofonoff and Millard, 1983; Feistel, 2003). For high-salinity brines and wide temperature and pressure ranges, empirical algorithms show a wide spread and must be viewed with caution (Adams and Bachu, 2002). However, theoretically well-founded extensions may be found on the basis of Pitzer's semi-empirical approach, as demonstrated for aqueous NaCl (Pitzer et al., 1984; Archer, 1992). Also for pure $CO_2$ an equation of state has been validated for a sufficiently wide P-T range (Ely et al., 1989; Pitzer and Sterner, 1995). For the binary $CO_2$-$H_20$ and ternary $CO_2$-$H_20$-NaCl systems, data and models have been reviewed by Hu et al. (2005). These authors conclude that presently available models and data sets are not consistent and that this poses some limits on the detailed modelling of $CO_2$ sequestration in reservoirs. These restrictions are not that severe for the limited PVTx-regime in the ocean, however.

$CO_2$ may occur in seawater in the pure gaseous and liquid phases and in dissolved form. It may also occur as a clathrate hydrate, where a cubic solid lattice of water molecules encloses gas molecules of $CO_2$ (v. Stackelberg, 1949; Miller, 1961; Sloan, 1998; Buffett, 2000). Hydrates look like ice and have a similar density, yet the gas molecules are trapped in water cages at two orders of magnitude larger concentration than in the gas form. The stability of the hydrate, in dependence on pressure, temperature and solute content, is of major interest to understand dissolution processes in seawater and marine sediments.

## 2.1 Density and equation of state

Figure 5 shows the density regimes of liquid $C0_2$, seawater and $CO_2$-saturated seawater relevant in the ocean. The transition pressure between the gaseous and liquid phases is normally reached at 400-500 m depth (Figure 6). Due to its higher compressibility liquid $C0_2$ becomes, for typical oceanic temperatures, denser than seawater below $\approx$ 3000 depth. $CO_2$-saturated seawater is considerably denser than seawater. This density difference exceeds the typical density differences that drive the ocean-circulation by an order of magnitude.

The seawater density increase due to dissolution of $CO_2$ may be approximated by a linear concentration dependence (Bradshaw, 1973), and such an equation of state has been used in oceanic simulations (Fer and Haugan, 2003; Haugan and Alendal, 2005). For the temperature range 3 to 12 ℃, and a pressure up to 12 MPa (1200 m ocean depth), this assumption appears to be justified (Song et al., 2005). As mentioned above, models and observations are less conclusive over the full PVTx range that needs to be considered for storage in subsea formations, and a sufficiently accurate equation of state has still to be established for these regimes (Hu et al., 2005).

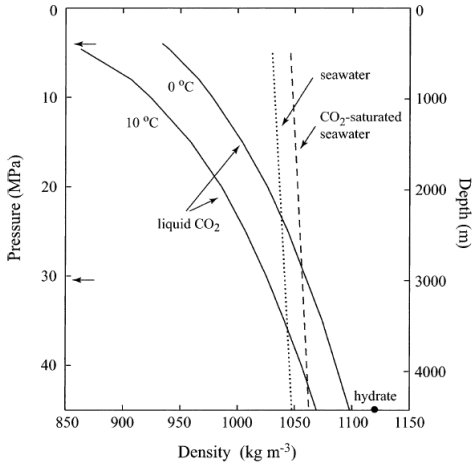


Figure 5: Density of liquid $C0_2$, seawater and $CO_2$-saturated seawater (for 5 ℃) versus pressure. Arrows indicate the typical oceanic transition levels to the gas (upper) and hydrate (lower) phases. From Fer and Haugan (2003).

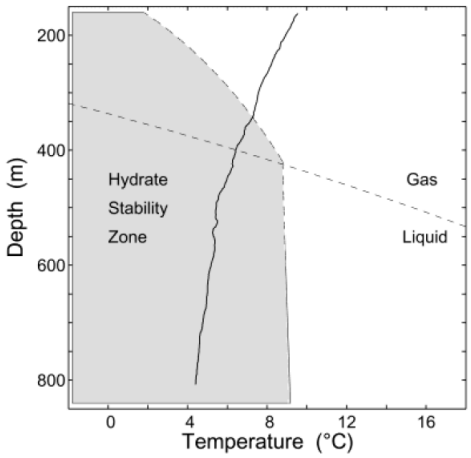


Figure 6: Phase equilibrium depth-T diagram of $C0_2$ along with a typical upper-ocean temperature gradient (solid curve). From Brewer et al. (2002).

## 2.2 Solubility

For the PTSx-range of interest in the ocean and seabed, solubility of $CO_2$ decreases with temperature and composition and decreases with pressure (Figures 7 and 7). Models and observations of the solubility of $CO_2$ in water and aqueous solutions have been reviewed by Duan and Sun (2003). These authors applied Pitzer's ion interaction approach to model $CO_2$ solubility in seawater for temperature of 273 K and pressures down to 2000 bar and have recently improved the computations and accuracy Duan et al. (2006).

## 2.3 Diffusion and dissolution

Dissolution depends on the concentration gradient at an interface via Fick's law

$$F_s = D_s(\frac{dC}{dz})_{int}, \tag{1}$$

where $D_s$ is the molecular diffusivity of a dissolved species with concentration $C$. For the applications relevant in the present study the interfacial gradient is normally controlled by convection and a function of the saturation concentration $C_{sat}$ (from solubility), a concentration $C_\infty$ far from the interface, and the convecto-diffusive mass transport $V_*$. It is frequently parametrised as $D_s(dC/dz)_{int} = V_*(C_{sat} - C_\infty)$. $V_*$ depends on the hydrodynamics near the interface and scales as some function of the molecular viscosity $\nu$ and the Schmidt number $Sc = \nu/D_s$.

Some diffusion coefficients for $CO_2$ and other gases and ions are listed in Figure 9. Note that the viscosity of water decreases for the range 0 to 20

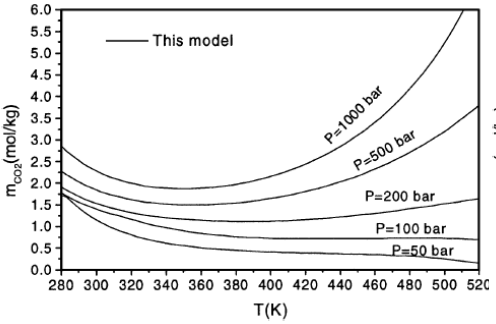


Figure 7: Solubility of $CO_2$ in pure water. From Duan and Sun (2003).

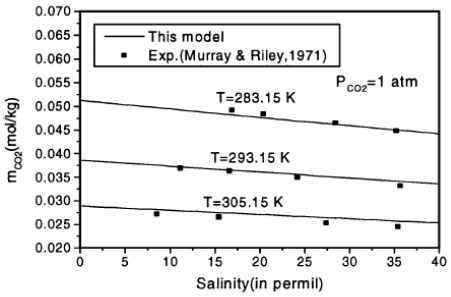


Figure 8: Solubility of $CO_2$ in seawater. From Duan and Sun (2003).

℃ by a factor 1.8 (IAPWS, 2003; Zaytsev and Aseyev, 1992). These values are consistent with classical thermodynamics and the Stokes-Einstein relation which implies $D_s \sim \theta/\mu$, where $\theta$ the absolute (Kelvin) temperature and $\mu$ the dynamic viscosity $\nu\rho$. As $\mu$ decreases with temperature and $D_s$ increases with $\theta$ and $1/\mu$, the Schmidt number depends considerably on temperature. This has often been ignored in studies to be mentioned below and needs to be properly accounted for in models of interface dissolution enhanced by convective transport.

## 2.4 Hydrate formation and stability

At pressures higher than the gas-liquid-hydrate equilibrium (at 433 m) the phase equilibrium between liquid $CO_2$ and gas hydrate shows a weak pressure dependence (Figure 6). Thermodynamic predictions of this stability curve for gas hydrate based on Pitzer's method have been presented for seawater by Duan and Sun (2006). According to this model the equilibrium temperature increases with depth from 8.43 ℃(433 m) to 10 ℃(1874 m) and 11 ℃(3171 m). In oceanic intermediate and deep regimes $CO_2$ may thus, under appropriate saturation conditions, be present in form of hydrates.

The density and composition of hydrates depends on pressure (Handa, 1990; Sloan, 1998). Observations at deep ocean conditions of 30 MPa indicate an expected range of 1.09 to 1.11 g/cm$^3$ (Aya et al., 1997). The hydrate density 1.12 g/cm$^3$ indicated in Figure 5 is based on a structural X-ray diffraction study at a comparable high pressure (Udachin et al., 2001). While the thermodynamics of hydrate formation is reasonably understood, the role of kinetics and interfacial processes in determining the exact composition, microstructure and density of hydrates is still a challenge for future research (Sloan, 1998, 2004).

## 2.5 Oceanic hydrate stability regimes

The general picture of hydrate stability in the deep ocean is indicated in figure 10. In the ocean temperatures decreases towards the bottom, and under most conditions one enters the hydrate stability regime below 300-400 m depth. Near-bottom temperatures of 0 to 5 ℃ imply, with a geothermal gradient of $\approx 0.05K/m$, a regime of 100-200m below sea bottom, where $CO_2$ would be

**Table 14.1** Molecular diffusion coefficients of representative gases, ions, and molecules dissolved in seawater (units of $10^{-5}$ cm$^2$ s$^{-1}$)[a].

| Species | 0°C | 5°C | 10°C | 15°C | 20°C |
|---|---|---|---|---|---|
| $O_2$ | 1.00 | 1.23 | 1.46 | 1.69 | 1.91 |
| $CO_2$ | 0.84 | 1.03 | 1.22 | 1.41 | 1.60 |
| $H_2S$ | 0.92 | 1.13 | 1.34 | 1.55 | 1.75 |
| $H^+$ | 5.17 | 5.89 | 6.60 | 7.30 | 8.01 |
| $Na^+$ | 0.58 | 0.72 | 0.85 | 0.99 | 1.12 |
| $NH_4^+$ | 0.93 | 1.10 | 1.29 | 1.47 | 1.66 |
| $Ca^{2+}$ | 0.34 | 0.43 | 0.51 | 0.59 | 0.67 |
| $OH^-$ | 2.46 | 2.97 | 3.48 | 3.98 | 4.47 |
| $Cl^-$ | 0.91 | 1.12 | 1.32 | 1.52 | 1.72 |
| $NO_3^-$ | 0.90 | 1.08 | 1.26 | 1.44 | 1.62 |
| $SO_4^{2-}$ | 0.46 | 0.57 | 0.68 | 0.79 | 0.89 |
| Acetate | 0.46 | 0.57 | 0.68 | 0.80 | 0.91 |
| Lactate | 0.42 | 0.53 | 0.64 | 0.75 | 0.86 |

[a] After Boudreau (1997) and Schultz (2000)

Figure 9: Molecular diffusion coefficients of several gases, ions and molecules. From Jørgensen (2001).

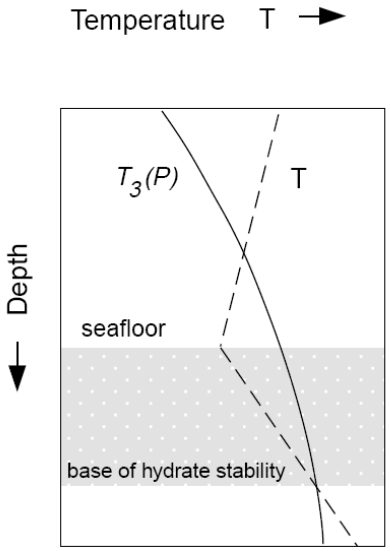


Figure 10: Principal regimes of hydrate stability in the ocean. From Buffett (2000).

present in form of hydrate. Only at deeper levels it is expected in its stable liquid form. For somewhat different pressure and temperature ranges the problem also applies to methane hydrate stability, for which the phase transition has been recognised as a possible driver of climate change (Kvenvolden, 1993). Some further remarks on this problem are given in section 3.2 below. Conditions that prevail in warm shallow seas are thermodynamically different: if temperatures are low enough for hydrates to form, the transition will be from the gaseous to the hydrate phase (Figure 6).

The hydrate stability conditions are important in terms of phase transitions and permeability of the seabed. In the ocean hydrate will under most cases only be metastable, as its stability requires saturation. As will be discussed in the following section 3, the details of this metastability are rather challenging in the dissolution problem of rising $CO_2$ droplets covered by a hydrate shell.

# 3 Phase transitions and metastability

## 3.1 Droplets with hydrate shells

Observations of the rapid formation of hydrates in containers at large ocean depths have been published by Brewer et al. (1999). It has also been documented that $CO_2$ and methane droplets released in the oceanic hydrate stability regime become covered with a thin hydrate shell, while their buoyancy is still governed by the density of liquid $CO2$ (Brewer et al., 2002). Sugaya and Mori (1996) proposed that the detailed morphology of such a hydrate layer depends strongly on the degree of supersaturation, and thus the hydrodynamic conditions adjacent to the interface. In laboratory experiments the latter authors estimated a hydrate layer thickness of $\approx 10\mu$m based on optical observations. To explain such a shell, Mori and Mochizuki (1997) have suggested a perforated plate model from which a hydrate thickness in dynamic equilibrium between dissolution and dissociation can be predicted. The thickness $\delta_{sh}$ may be written as

$$\delta_{sh} = \frac{r_c \phi \gamma_{w,co2}}{4\tau^2 V_* \mu} F(C_{sat}, C_\infty, n), \tag{2}$$

with capillary radius $r_c$, porosity $\phi$, tortuosity $\tau$, liquid $CO_2$-water interfacial tension $\gamma_{w,co2}$, kinematic viscosity $\mu$ and a function $F$ that depends on solubility $C_{sat}$, ambient dissolved concentration $C_\infty$ and hydration number $n$. The main point is the dependence on unknown structural parameters like the porosity, pore radius and tortuosity, as well the mass transfer rate $V_*$ at the hydrate-water interface. Due to the lack in mass transfer information in the laboratory experiments made by (Sugaya and Mori, 1996), it was not possible to constrain the model parameters (Mori and Mochizuki, 1997). A number of alternative models and explanations have been discussed by Mori (1998). He concluded that the perforated plate model was one of the most realistic physical explanations for the stability of a thin hydrate shell.

An approach to estimate the plate thickness by a mechanistic approach, based on correlation with observed droplet rise and dimensions (Gabitto and Tsouris, 2006) has been criticised by Mori and Murakami (2007). It is worth a note that in the perforated plate model the hydrate shell has no direct insulating influence on the dissolution rate (Mori, 1998; Mori and Murakami, 2007), yet the reduction comes from a change in solubility in the presence of hydrate (Zhang, 2005). The thickness may, however, be of interest when considering the elasticity and deformation of the film. In a different context, considering a lake of $CO_2$ covered by hydrate, Fer and Haugan (2003) have speculated on the possibility of tensile fracture leading to the instability of such shell. Replacing the liquid-liquid surface tension in a hydrodynamical problem by the tensile strength of the hydrate layer, these authors calculated the most instable wave length and critical interface velocities for the layer break-up.

Under large enough supercoolings hydrates form with a dendritic structure as known for ice, which has been shown by optical observation methods (Ohmura et al., 2004; Katsuki et al., 2007), yet there are at present no observations that could validate the porous structure of hydrate shells forming in the oceanic

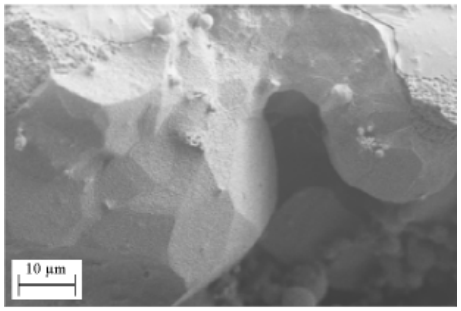


Figure 11: FE-SEM image of $CH_4$-gas hydrate grown at 264 K and 60 bar. From Staykova et al. (2003).

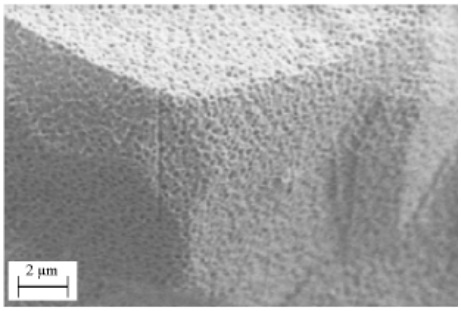


Figure 12: Submicron structure of $CH_4$-gas hydrate grown at 264 K and 60 bar. From Staykova et al. (2003).

environment with submicron resolution, as assume by (Mori and Mochizuki, 1997). However, the PT-regime where hydrate forms from the ice phase is accessible in the laboratory. Microstructure observations performed to date and reveal a number of results that may be relevant for the hydrate shell problem Kuhs et al. (2000); Staykova et al. (2003); Klapproth et al. (2003); Stern et al. (2004); Genov et al. (2004), as they agree remarkably with hydrates found in nature (Kuhs et al., 2004; Stern et al., 2004). In particular it was found by Kuhs et al. (2000) that $CO_2$ hydrate grown from the ice phase is a structure with porosity of 10-20% and pores with diamters of 20 to 100 nm. Methane hydrate had almost an order of magnitude wider pores. Using these numbers in the model from (Mori and Mochizuki, 1997), one would obtain a hydrate film thickness of $\approx$ 1 mm for a typical rising or flow velocity of $\approx$ 0.1 m/s, if interfacial fluxes are based on the hydrodynamical scalings used by Fer and Haugan (2003). Notably, this thickness is two orders of magnitude larger than one obtains on the basis of a low porosity of 0.1%, the value assumed in studies by Mori and Mochizuki (1997) and Fer and Haugan (2003).

A shell thickness of 1 mm is inconsistent with observations. It would imply that droplets in the field study by Brewer et al. (2002) should not have been rising as they did. To yield a value of the order of 10 $\mu$m, as estimated by Sugaya and Mori (1996), one would have to assume that only a small fraction of the pores is interconnected. Indeed, observations made by Kuhs et al. (2004) seem to indicate this constraint. These authors report that the pores are predominantly closed and thus only accessible at the surface. Such observations suggest another idea. It is that not the pore structure and the mass transfer control the film thickness, yet that the film thickness is controlled by growth kinetics and diffusive transport at its surface. The connectivity of the pores might then adjust to these conditions instead of primarily constraining them. Dynamical length scales of the order of some ten micrometers have been reported in two studies: Stern et al. (2005) reported that during re-texturing many hydrate grains developed into hollow shells, typically 5 to 20 microns thick, while Stern et al. (2004) mentioned a *hydrate rind* of 5 to 30 microns as an initial scale for hydrates that formed from melting ice.

Recently, rejecting the perforated-plate model, it has been proposed that the mass transfer from the hydrate shell is balanced by a diffusive flux of $CO_2$ through the hydrate layer, driven by a hopping mechanism (Radhakrishnan et al., 2003). This approach, for which the authors adopted the shell diffusivity of $CO_2$ predicted in molecular dynamics simulations by (Demurov et al., 2002), appears to give the correct order of magnitude of the shell thickness for some experiments. However, the data available so far are very sparse and cannot be viewed as a validation. The length scale of several tens of micrometer that the model predicts also appear in a number of other observations on porous hydrates mentioned above. This points to the importance of modelling and imaging of microstructure formation of hydrates, to date an open field of research. Recently it has been reported that a $CO_2$-hydrate lake may exist at depths where liquid $CO_2$ is lighter than seawater, if it is covered by a pavement layer (Nealson, 2006). In this case the hydrate layer was rather thick, of the order of 10 cm, yet contained bacteria and other substances from the sediment. Interpretation of this regime, and other natural samples, requires a proper chemical and structural analysis on the submicrometer scale.

Besides the mentioned observations of microstructure of hydrates growing from the ice phase (and thus accessible to a number of observational methods), first basic thermodynamic phase field simulations of hydrate growth have been performed (Svandal et al., 2006), indicating future possibilities to understand different hydrate morphologies. Also the tensile strength of hydrate films has been measured for different pressure and temperature regimes (Yamane et al., 2000). Indirect derivations of and effective tensile strength of the hydrate layer in a deep sea experiment have been proposed based on hydrodynamic stability theory (Hove and Haugan, 2005). The strength was found to be of the order of the liquid $CO_2$ and hydrate-water interfacial energies. A strong abnormal behaviour of the strength close to the dissociation temperature has been reported by (Yamane et al., 2000) and also Tewes and Boury (2004) observed a dynamical response of liquid $CO_2$-$H_2O$ interface energy during increasing pressure.

In conclusion, there is much progress going on to elucidate the physical processes related to hydrate formation in the environment. However, a proper description in applied sciences, to produce a better understanding of the diffusive, kinetic processes and possibly hydrodynamical processes during the formation of porous gas hydrates, still requires a lot of fundamental work. This work must be highly multidisciplinary, linking microscopic and macroscopic observations and models.

## 3.2 Hydrates in porous media

The understanding of the hydrate stability regime, implied by the hydrothermal and geothermal gradients near the sea floor (Figure 10) has given rise to a discussion of its role in terms of longterm climate changes, driven by catastrophic release of the strong greenhouse has methane (Kvenvolden, 1993; Wefer et al., 1994; Dickens et al., 1995; Nisbet, 2002; Zhang, 2003). The mechanisms are clear from Figure 10: The instability of hydrates in the sediments can be reached by both warming of the ocean or, a mechanism that will be dominant in shallow

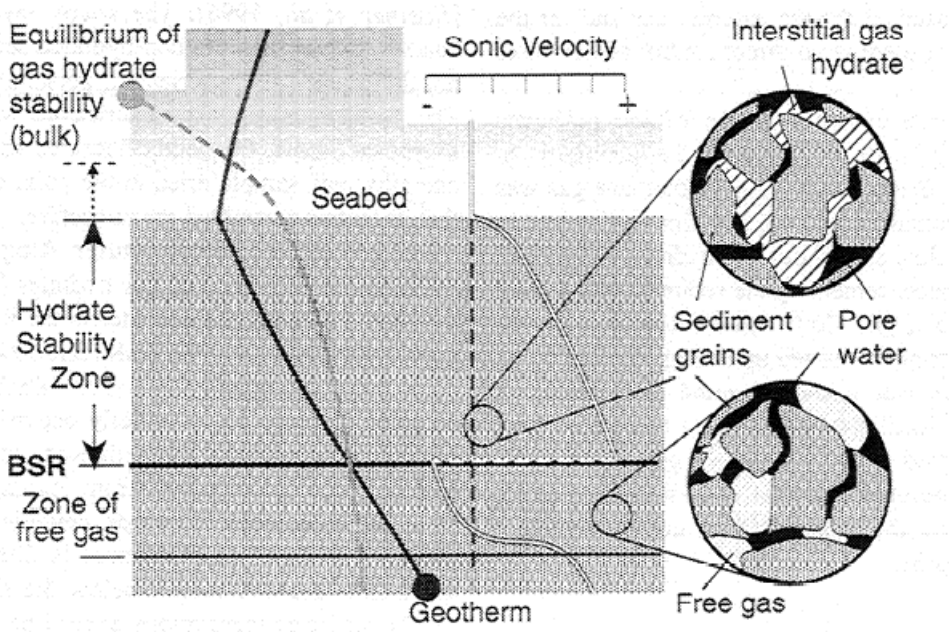


Figure 13: A conventional model for the sealing of pores by hydrates in the stability zone close to the seafloor. From Clennell et al. (1999).

seas, a decrease in sea level (and bottom pressure).

A conventional view of the role of hydrates in marine sediments is illustrated in 13. The hydrates may be thought to fill the pores of sediments, making them impermeable to liquid and gas fluxes from the lower layers (Kvenvolden, 1993; Clennell et al., 1999; Henry et al., 1999; Østergård et al., 2002). Hydrate stability may thus also be viewed as a relevant condition in connection with the safety of $CO_2$ storage.

The idea brings about another question. If $CO_2$ approaches the seafloor from below, will it be transformed into hydrate, thereby stopping its leakage by self-sealing? Two mechanisms relevant to answer this question will be discussed as follows.

### 3.2.1 Gibbs-Thomson effect

Freezing of a non wetting liquid in small capillaries is controlled by the Gibbs-Thomson relation. It gives the freezing point depression $\Delta_T$ in dependence on the capillary radius $R$ as

$$\Delta T_\Gamma = \frac{2\Gamma}{R}, \tag{3}$$

where $\Gamma = T_m\gamma/L_v$ is the Gibbs-Thomson parameter, $\gamma$ being the solid-liquid surface free energy, $L_v$ the volumetric latent heat of fusion, $T_m$ the melting point in Kelvin. For pure water/ice $\Gamma \approx 2.7 \times 10^{-8}$ m K which implies a freezing point depression of 1.08 K for a pore of 100 nm diameter. Relation 3 has been classically used to determine the interfacial free energy of the ice-water

system, e.g., Hillig (1998). Uchida et al. (2002) derived 29 mJ/m$^2$ for ice and determined values of 17 mJ/m$^2$ and 13 mJ/m$^2$ for $CH_4$ and $CO_2$, respectively. Anderson et al. (2003a) proposed that during melting experiments one should use equation 3 with the factor of 2 missing on the right hand side. The latter authors then obtained very similar values of $32 \pm 2$ mJ/m$^2$, $32 \pm 3$ mJ/m$^2$ and $30 \pm 3$ mJ/m$^2$ for ice, $CH_4$ and $CO_2$, respectively. They further argued that the data for ice reported by Uchida et al. (2002) might have been in error due to the presence of a broad pore size distribution. A difference between $\gamma$ obtained during melting and freezing in pores has been reported earlier (Ishikiriyama et al., 1995). Considering the available data it seems most plausible to assume a smaller $\Gamma \approx 1.8 \times 10^{-8}$ m K in equation 3, when melting is considered. In general, it can be concluded that $\Gamma$ is very similar for ice and gas hydrates.

An example of interpretation of field data in terms of equation 3 is shown in Figure 14 It shows cumulative pore size distributions derived by mercury injection into samples from Blake Ridge, taken near the basis of the hydrate stability zone. The 'percolation threshold' given by the inflection point may be interpreted as the lower limit of pore throat radii that determines the permeability. This approach is based on the critical path analysis (CPA) of heterogeneous media, which assumes that flow is primarily taking place through the larger channels (Thompson et al., 1987). The 'percolation threshold' marks the fraction of the overall porosity where the pore space becomes interconnected, notably taking a value of $\phi_c \approx 10$ % (in terms of absolute porosity) for these samples. The interpretation of Figure 14 on the basis of the above mentioned $\Gamma$ is that both methane and $CO_2$, permeating through the base into the hydrate stability zone, would not experience a stability temperature depression of more then 0.6 K. Such a limit has been pointed out by Henry et al. (1999) by using ice-water interfacial energy values.

Modelling and interpretation of hydrate stability in connection with natural pore size distributions, considering effects of dissolved salts, have been performed (Østergård et al., 2002; Anderson et al., 2003b) with a recent application to marine sediments (Sun and Duan, 2007). A laboratory study of the morphology of hydrate growth in a porous medium in dependence on the supercooling between 3.4 and 14 K, showing dendritic growth at lowest supercoolings, was performed by Katsuki et al. (2007).

### 3.2.2 Metastability: Undercooling and Superheating

A second aspect of hydrate stability in porous media is related to nucleation. For the ice-water system it is well known that freezing above the homogeneous nucleation temperature of $\approx -40$ ℃requires the presence of nuclei, e.g., Hobbs (1974); Pruppacher and Klett (1997). High supercooling of water can be realised in emulsions, as the separation into many small volumes limits the probability of activation of nuclei. A similar principal morphology is given in porous media and has been investigated by Zatsepina and Buffett (2001) for $CO_2$-hydrate. These authors interpret resistance measurements during cooling and warming of water solutions with dissolved $CO_2$ in a porous medium of grain size 0.4-0.6 mm. Nucleation of both vapour and hydrate during crossing of the three-phase-

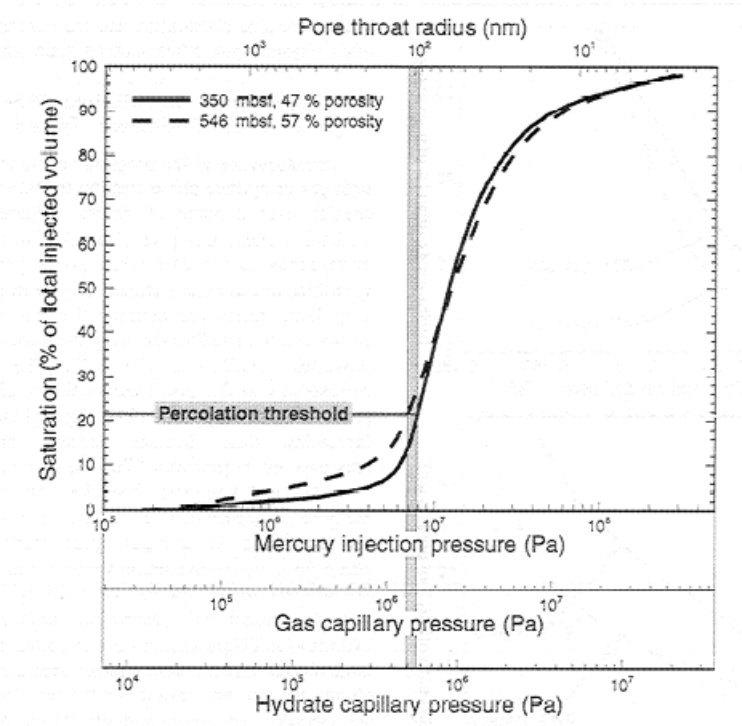


Figure 14: Cumulative pore size distribution derived by mercury injection. The 'percolation' threshold given by the inflection point may be interpreted as the lower limit of pore throat radii that determines the permeability. From Henry et al. (1999).

stability temperature (Figure 16) was associated with plots as shown in Figure 15. It was found that superheating and supercooling by 3-4 K was possible, before the phase-transition took place.

Henry et al. (1999) pointed out that an observed shift in the hydrate stability base temperature by 1-2 K cannot be explained by pore size effects via the Gibbs-Thompson relation. In a statistical nucleation model, parametrised on the basis of their experiments, Zatsepina and Buffett (2003) predicted that nucleation of hydrate in pores of 100 nm radius would, even for supercooling of 5 K, take $10^9$ years. These observations indicate the possible delay of nucleation when gas-bearing water rises into the hydrate stability zone.

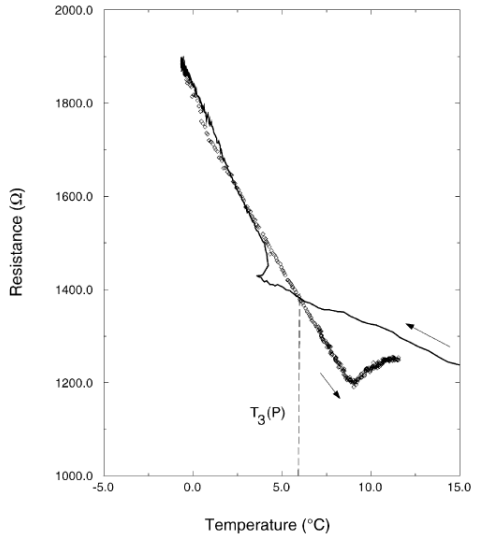


Figure 15: Resistance measurements during cooling and warming of $CO_2$ in a porous medium of grain size 0.4-0.6 mm, P= 2.6 MPa and $T_3(P) = 6.1$ ℃, indicating superheating and supercooling prior to nucleation. From Zatsepina and Buffett (2001).

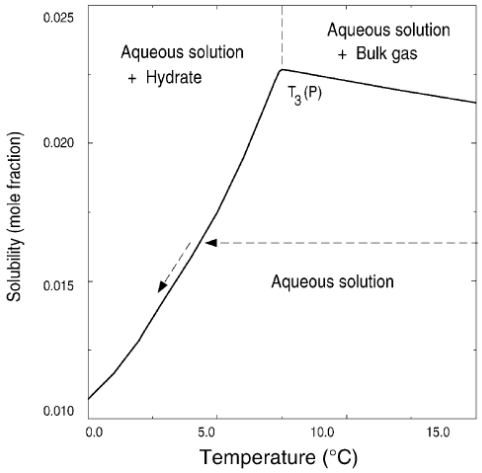


Figure 16: Phase diagram of $CO_2$-$H_20$ mixture at constant pressure 3 MPa, corresponding to the experiment in figure 15. From Zatsepina and Buffett (2001)

# 4 Droplet dynamics and thermodynamics

When a droplet or gas bubble of $CO_2$ moves through undersaturated seawater it will dissolve. At the same time a rising (sinking) gas bubble expands (contracts), an effect that is opposite to the volume change by dissolution. The velocity $V$ of perfectly spherical noninteracting droplets due to buoyancy may be written in the form

$$V = \left(\frac{8}{3}\frac{gr\rho'}{C_d}\right)^{1/2} \tag{4}$$

where $\rho' = (1 - \rho_{CO2}/\rho_{sw})$ is the buoyancy of $CO_2$ in seawater, $r$ the radius of a droplet and $C_d$ the drag coefficient. This equation is obtained by equating buoyancy force $(4/3\pi r^3(\rho_{sw} - \rho_{CO2})g)$ with a quadratic drag force due to the effective cross-sectional area, $(\pi r^2 C_d V^2 \rho_{sw}/2)$. It is valid for spheres, and in a more general form one must use the cross-sectional area normal to the flow in connection with the volume of the body. Equation 4 is in principle the definition of an effective drag coefficient $C_d$ (Davies and Taylor, 1950; Levich, 1962; Batchelor, 1967), which either has to be found from theory or observation. The velocity $V$, in the steady state when forces balance, is often termed the *terminal velocity.*

### 4.1 Low Reynolds number flow

At low Reynolds numbers, for $Re = 2RV/\nu < 1$ (and thus for very tiny droplets), the classical Stokes-flow relation for a solid sphere (Levich, 1962; Batchelor, 1967) gives

$$V = C\frac{2}{9}\frac{gr^2\rho'}{\nu}, \qquad C_d = \frac{24}{Re} \tag{5}$$

and a dependence of $V \sim r^2$. In the derivation of the Stokes equation inertia forces are neglected and buoyancy is balanced by friction. The shape factor C is 1 for a sphere and decreases with specific surface area, taking for example the value of 0.921 for a cube (Clift et al., 1978; Happel and Brenner, 1986). When the droplet or bubble has no infinite viscosity, a more realistic equation is the Rybczynski-Hadamard formula (Levich, 1962; Batchelor, 1967), which for a sphere (setting $C = 1$) may be written as

$$V = \frac{3 + 3k_\nu}{2 + 3k_\nu}\frac{2}{9}\frac{gr^2\rho'}{\nu}. \tag{6}$$

Here $k_\nu$ is the ratio of the dynamic viscosity ratio of the droplet to that of the fluid. For a solid particle ($k_\nu = \infty$) it passes into the Stokes equation 5. For a gas ($k_\nu << 1$) it gives a 3/2 larger velocity $V$ and a lower drag $C_d = 16/Re$ than the Stokes flow. The difference relates to the difference in the surface mobility of a solid and a low-viscosity droplet (Levich, 1962; Moore, 1963; Batchelor, 1967). The observations that gas bubbles sometimes behave according to Stokes law has been explained in terms of surface-active substances that let the bubble behave like a solid (Levich, 1962; Batchelor, 1967). As liquid $CO_2$ has a more than an order of magnitude lower viscosity than seawater, equation 6 should be applicable, with a prefactor close to 3/2. The low Reynolds number Stokes limit has been discussed in terms of settling velocities of (solid) sediments (Lerman, 1979).

### 4.2 High Reynolds numbers

To include inertial effects one may consider sufficiently large gas bubbles that rise at high enough $Re$, to let boundary-layer ideas become applicable, but still small enough $Re$ to keep their spherical shape. Assuming a free boundary condition one may then obtain the solution $C_d = 48/Re$ (Levich, 1962; Batchelor, 1967; Clift et al., 1978) which is two times the Stokes drag. Implementing boundary theory leads to the solution (Moore, 1963; Batchelor, 1967)

$$C_d = \frac{48}{Re}(1 - \frac{2.21}{Re^{1/2}}), \tag{7}$$

which has later been derived including higher order terms (Kang and Leal, 1988). The terminal velocity is thus half the Stokes velocity from equation 5. The treatment of the inner boundary layer of the droplet is more difficult and several approaches have been made to refine equation 7 in terms of viscosity and density ratios (Clift et al., 1978). A detailed discussion of many aspects of the problem was given by Harper (1972).

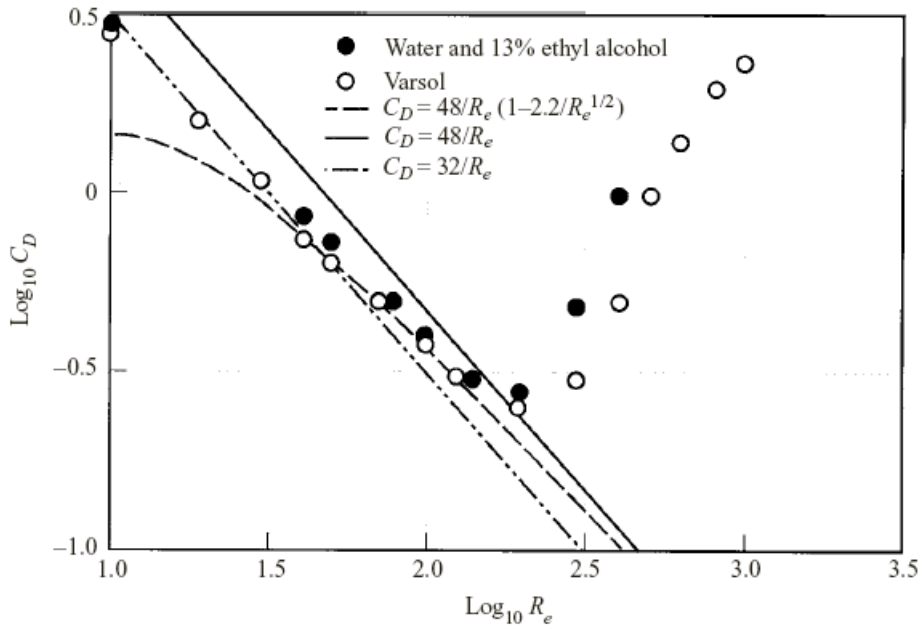


Figure 17: Drag coefficient of bubbles in dependence on the Reynolds number. From Joseph (2003) after Batchelor (1967).

Equation 7 is valid for undeformed spherical gas bubbles at high $Re$, while at low $Re$ equation 6 becomes valid, yielding a three times smaller limiting $C_d = 16/Re$. The low $Re$-limit is in agreement with observations (Clift et al., 1978; Bhaga and Weber, 1981). However, at $Re$ above $\approx 100$ it starts to fail. Up to $Re \approx 300 - 500$ the flow is typically characterised by a quasi-constant drag, with a sharp increase at larger $Re$ (Batchelor, 1967; Clift et al., 1978; Maxworthy et al., 1996), see Figure 17. This can be understood in terms of the deformation from a spherical shape and compares to the onset of wake instability in the case of rigid spheres, taking place at $130 < Re < 400$ (Clift et al., 1978). However, solid spheres experience a much smaller variation in $C_d$ at high $Re$ and a standard drag curve compiled from many data sources indicates a value $0.4 < C_d 0.5$ for a wide range of $500 < Re < 10^5$. A value of $C_d = 0.445$ has been mentioned by Clift et al. (1978) as most reasonable approximation.

Furthermore it is important to note, that experiments have shown that rigid discs and spheroids have a larger $C_d$ by a factor 2 to 3 when aspect ratios become large (Clift et al., 1978).

The case of liquid and gas bubbles, which begin to deform at high Reynolds numbers, is more complex. The dependence of the the drag coefficient on shape and flow conditions is, in addition to $Re$, often described in terms of two other non-dimensional numbers that include the surface tension $\sigma$: The Morton number $Mo = g\nu^4\rho_{sw}^3/\sigma^3$ and the Eötvös number $Eo = g(2r)^2(\Delta\rho)/\sigma$ (Moore, 1959; Harper, 1972; Clift et al., 1978). Small deformations are, for example, given in a liquid of small $Mo$ when bubbles rise at moderate $Re$, because surface tension

keeps the circular shape. For low Morton number systems ($< 10^{-8}$) like water, the shape of bubbles changes with increasing $Re$ from spherical to increasingly oblate, then fluctuates, until they take the form of an umbrella, steady at its front even if the rear fluctuates (Moore, 1959; Clift et al., 1978). Much progress in the understanding of these umbrellas or spherical caps has been made by Davies and Taylor (1950) in their famous study. On the one hand these authors showed that the velocity of spherical caps can be described by a stagnation-point condition

$$V = \left(\frac{4}{9} g \rho' r_0\right)^{1/2}, \tag{8}$$

where $r_0$ is the radius of curvature at the tip of the spherical cap. On the other hand they also showed that the drag coefficient based on $C_d = g\mathcal{V}/(1/2V^2F)$, with maximum cross-sectional area $F = \pi r_\perp^2$ transverse to the flow, and bubble volume $\mathcal{V}$, was close to unity for the spherical cap bubbles. Davies and Taylor (1950) further pointed out their experiments strongly supported the geometrical similarity of spherical cap bubbles and a constant $C_d$. Their experiments have been later confirmed and interpreted by many authors in terms of the relation

$$C_d = \frac{8}{3} \frac{g \rho' r_e}{V^2} \approx \frac{8}{3} \tag{9}$$

for the drag coefficient of spherical cap bubbles at large $Re$, which is now based on the equivalent radius $r_e = (3\mathcal{V}/4\pi)^{1/3}$ (Moore, 1959; Harper, 1972; Clift et al., 1978; Bhaga and Weber, 1981; Joseph, 2003). The limiting velocity is thus

$$V \approx \left(g \rho' r_e\right)^{1/2}. \tag{10}$$

once the regime of spherical cap bubbles has been reached.

The described regimes are summarised in Figure 18. It is seen that, in dependence on bubble rigidity and $Re$, a wide number of drag coefficients is possible. For gas bubbles in water Figure 19 illustrates the intermediate regime between spherical and spherical-cap drag, where the rise velocity is relatively constant over a wide range of Reynolds numbers. Algorithms for particular regimes of fluid properties and shapes may be found in the standard work by Clift et al. (1978). A number of more recent algorithms was discussed by Kalbaliyev and Ceylan (2007), who proposed a preferred set of equations for the prediction of $C_d$ for the solid sphere and gas bubble regimes.

The behaviour in Figures 18 and 19 may be approximated by parameterising the shape of particles in terms of $Re$, $Mo$ and $Eo$. A number of such approaches have been made, but in particular at high Re, when secondary motion exist, the problem is not well understood (Clift et al., 1978) and the complexity is indicated by the role of contamination in Figure 18. In this sense any suggested algorithm that is not based on coupled flow and shape simulations, like the recent ones by Kalbaliyev and Ceylan (2007) or Bozzano and Dente (2001), must be viewed with caution.

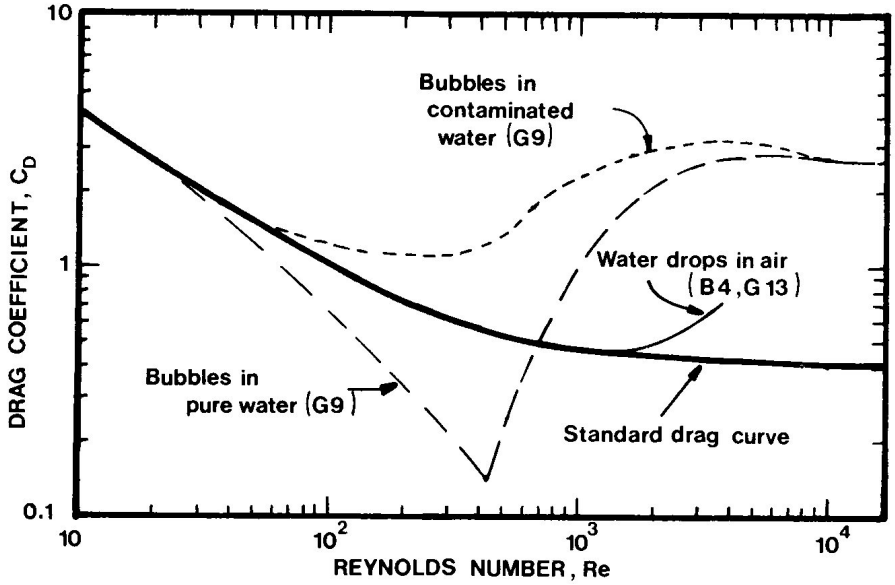


Figure 18: Comparison of standard drag curve (solid spheres), $C_d$ for bubbles in pure solutions and when influence by surface effects due to contamination. From Clift et al. (1978).

### 4.3 Turbulent mass diffusion and dissolution

The complexity and lack of universal solutions for the flow field indicates, that the problem of dissolution from a droplet or crystal interface is not an easy task. The success of simplifying drag-laws is limited. A proper analysis involves more detailed boundary layer and interface flux modelling. In general, the prediction of the solute flux $F_s$ from a dissolving interface under conditions of convection is described by

$$F_s = D_s(\frac{dC}{dz})_{int} = V_*(C_{sat} - C_\infty). \tag{11}$$

For specific geometries it is convenient to write the solute flux velocity as $V_* = ShD_s/\delta$, in terms of a Sherwood number $Sh$ and a thickness scale $\delta$. The general problem is the prediction of the interfacial solute flux velocity scale $V_*$ by boundary layer modelling. Boundary layer theories for horizontal surfaces and confined geometries, e.g. Gebhart et al. (1988); Schlichting (2004), need to be properly modified for flow around objects. However, for regular objects like the sphere and not too large Reynolds numbers, the problem has been treated by many authors. Again, Levich (1962) has provided some theoretical groundwork and Clift et al. (1978) have discussed empirical relations and hydrodynamic scalings for different shapes and Reynolds number regimes, rigid objects and gas bubbles.

A second relevant mechanism in the problem is compositional free convection due to dissolving solute of a droplet. Convection introduces different length (and transfer velocity) scales than the flow due to the terminal velocity. Dissolu-

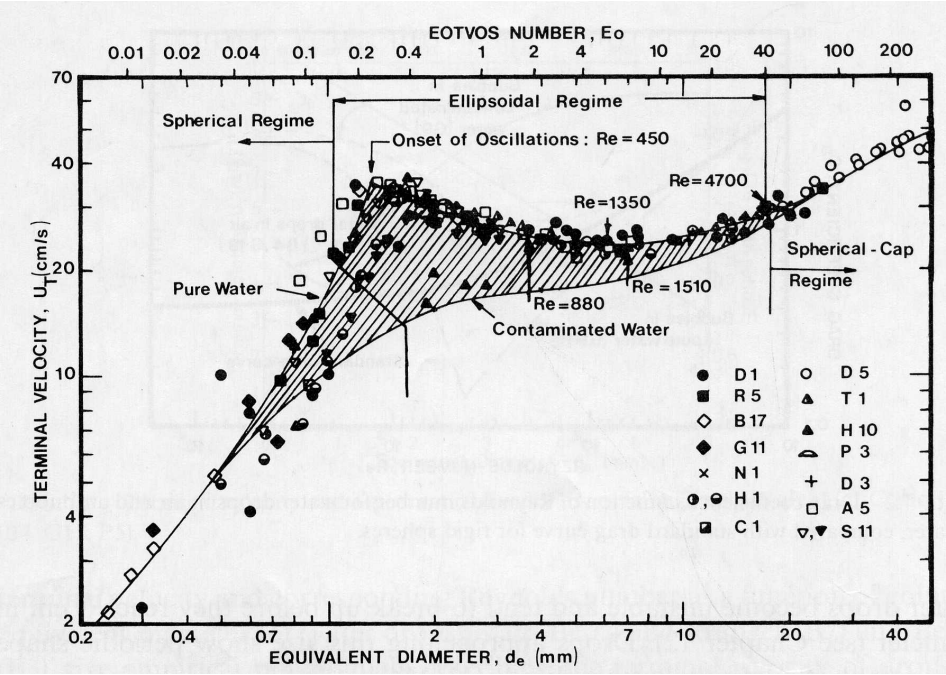


Figure 19: Terminal rise velocity for gas bubbles in water. From Clift et al. (1978).

tion driven by convection alone is reasonably understood for horizontal surfaces (Thomas and Armistead, 1968; Selman and Tobias, 1978; Kerr, 1994) in terms of classical theory of hydrodynamic instability (Chandrasekhar, 1961; Turner, 1973). Theory and experiment also exists for other geometries Gershuni and Zhukovitskii (1976); Selman and Tobias (1978); Gebhart et al. (1988). Also for free convection from the surface of spheres and arbitrary-shaped particles theories and scaling laws have been developed (Clift et al., 1978).

The problem becomes complex when both free convection (from the crystal or bubble interface) and forced convection (due to the crystal's terminal velocity) are present and interact, influencing both the terminal velocity and the dissolution. However, in the limiting cases of large and small $Re$, excluding situations where $Re \approx 1$, predictions and observations agree reasonably. For low $Re$, assuming Stokes flow, Kerr (1995) has found, in experiments with salt crystals, reasonable agreement with predictive equations from Clift et al. (1978). For $Re$ up to 350 Zhang and Xu (2003) also found reasonable agreement with theoretical scalings, by combining equations for drag, terminal velocity and solute flux given by Clift et al. (1978) for solid particles. The approach is expected to be valid to large Reynolds numbers $Re < 10^5$ and appears in reasonable agreement with the survival time of methane hydrate (Zhang and Xu, 2003) and observed diameters and dissolution rates of $CO2$ droplets surrounded by a hydrate shell (Zhang, 2005).

Due to the above discussion the application of dissolving bubbles, as suggested by Zhang and Xu (2003) and Zhang (2005), should be further critically

evaluated in terms of the following aspects: (i) while $C_d$ is affected by shape changes, the mass transfer and $Sh$ appears to be more independent of the latter (Clift et al., 1978) and it is critical to incorporate this into the analysis; (ii) the approach assumes a uniform equivalent boundary layer over the surface of a droplet, while the real concentration field will be much more complex with a compressed boundary layer in front of it; (iii) the dissolution from the surface of a droplet covered by a hydrate shell will depends on the porous structure and renewal of the shell and thus on processes that are not well understood yet.

### 4.4 Oceanic experiments and simulations

Some authors have applied equation 4 with a constant drag coefficient and a constant dissolution velocity to illustrate the levels to which gas or liquid droplets may rise a until they are dissolved (Holder et al., 1995; Clark et al., 2000).

The first dataset to analyse this problem was provided by Brewer et al. (2002) and also discussed on the basis of equation 4.[1] Droplets were released in the deep ocean and followed by an ROV to provide data on rise velocity and droplet radius. They found that the rise of a droplet could be closely described by equation 4 when using a constant $C_d = 1$ with a constant dissolution rate. The droplets were covered by a hydrate shell but irregular in form. From the above discussion it is recalled that $C_d \approx 0.45$ would be expected for a spherical droplet, but a factor of 2 to 3 larger $C_d$ is realistic for anisotropic shapes (Clift et al., 1978). In this sense the value $C_d = const$ is consistent with theory. However, a proper analysis would have to account for the detailed geometry of the followed feature, which actually was a droplet pair. As mentioned in the previous paragraph, Zhang (2005) provided a consistent simulation of the droplet rise rate and dissolution. The dissolution rate that he obtained by application of a simple forced convection algorithm (Clift et al., 1978) almost exactly matched the observations. However, the formula for the drag coefficient that he used was one for a spherical rigid droplet, which gives $0.47 < C_d < 0.62$ for the range $1000 > Re > 400$ typical for the experiment. His algorithm therefore should have slightly overestimated the rise velocity (a depth-time curve was not shown). In another study Gangstø et al. (2005) made predictions of the rise on the basis of the scalings from Bozzano and Dente (2001). The latter model however, as discussed above, should in principle only apply to gas bubbles, for which it parametrises the drag change with deformation at high $Re$. The assumed functional dependence of $C_d$ on $Re$ is therefore not physically justified, which may explain the poorer performance of the model by Gangstø et al. (2005) at low $Re$.

As shown by Gangstø et al. (2005), Brewer et al. (2002) only were successful in predicting the depth-time curve of droplets by assuming a constant drag and dissolution rate, while the constant drag predictions of the rise velocity alone did not give the observed behaviour. The better performance of the predictions by Gangstø et al. (2005) may indicate that despite a hydrate shell the droplets

[1]The authors use the incorrect expression $\rho' = (\rho_{sw}/\rho_{CO2} - 1)$ instead of $\rho' = (1 - \rho_{CO2}/\rho_{sw})$ and quote equation 4 as the 'Stokes velocity', which is neither correct.

behave like liquid or gas. This appears unlikely because, even if the hydrate shell is flexible, it may not promote shear to the inner of the droplets. It seems more likely that an inaccurate drag law is shaded by an inaccurate dissolution model, or that shape changes were accidentally taking place in a way that approaches this law. The many open questions indicate the need for more observations, proper evaluation of the geometry of droplets and, last not least, an evaluation of the role of the movement of the ROV, that may have stabilised the rise velocities. Such artificial effects, would be largest when the droplets are near the boundary of the ROV which, as pointed out by (Gangstø et al., 2005), might indeed have happened. The question was also raised by Mori and Murakami (2007).

The drag parametrisation used by Zhang (2005) has been criticised by Alendal et al. (2006) as giving 50 % too high rising velocities. It is, however, more realistic than a liquid-or gas bubble approach from Gangstø et al. (2005), and would, with an increase of the drag by a factor of 2-3 due to ellipticity of the droplets, perform reasonably well. To what degree the dissolution approach (Zhang and Xu, 2003; Zhang, 2005) needs to be modified due to assymetric boundary layer and droplet shape needs to be investigated. The model is a physically consistent treatment of surface renewal diffusion coupling that reproduces the observations well.

Another question that has been addressed is the reduction of dissolution rates by the presence of the hydrate shell (Aya et al., 1997; Ogasawara et al., 2001; Zhang, 2005; Gangstø et al., 2005). The explanation in terms of a different solubility in the presence of hydrate gives a quantitative correct reduction by a factor of $\approx 2$ (Zhang, 2005) for the dataset from Brewer et al. (2002). However, to what degree the dissolution may be affected by shape and surface mobility changes, needs also to be investigated. It seems plausible that a larger effective drag on a perturbed droplet will also enhance its dissolution. More recent data on rise velocities (Chen et al., 2003) indicate that also in the presence of a hydrate shell the shape of droplet changes to elliptical forms, with increasing drag and a terminal velocity plateau as seen in Figure 19. The droplets in the experiment discussed in the latter study were, however, strongly interacting. More proper evaluations of all effects on the drag are needed.

### 4.5 Future challenges

The above discussion indicates the future need of small-scale modelling of the flow, drag and dissolution of particles of different shapes. Some aspects are important for correct interpretation of existing and future studies. The application of a liquid droplet algorithm to predict $C_d$ (Gangstø et al., 2005), as it was also applied in a larger-scale study (Alendal and Drange, 2001), is not justified for rigid droplets with a hydrate shell. It gives a too large drag. On the other hand, also a non-spherical hydrate-shelled drop will experience some increase in the drag, and this increase and the typical shell geometry need to be established. If present, liquid $CO_2$ and seawater through which the latter rise have a viscosity ratio of the order of 10, and may thus reflect a case between gas and rigid bubbles. In any case, dissolution needs then to be modelled on the droplet

scale with high-resolution boundary layers. For non-dissolving particles a better understanding can be provided by numerical models. Both front-tracking approaches (Hua and Lou, 2007) and lattice Boltzmann simulations (Inamuro et al., 2004; Frank et al., 2006) have recently be applied to the problem, with realistic results on shapes.

There is a further need for the study of coagulation and droplet interaction. Boundary effects are known to become relevant when $d/D$, the ratio of droplet diameter to free flow path cross-sectional diameter, becomes larger than $\approx 0.1$ (Clift et al., 1978). With larger $d/D$ the effective drag increases while the rise velocity decreases. Similar results have been obtained by analytic approaches to bubble interactions (Zhang and Fan, 2003) and by numerical modelling of a swarm of bubbles (Krishna et al., 1999). Coalescence of bubbles and the accompanying shape changes may also be investigated by lattice Boltzmann simulations (Inamuro et al., 2004).

Finally, there should be a large potential to learn from other research fields that long have been treating analogous problems. Convective heat and mass transfer have been treated in the field of crystal growth (Tiller, 1991; Xu, 2004) and solutions found there may also serve as guides to further progress. In cloud physics many of the problems like droplet deformation, terminal velocity, droplet coagulation and diffusional growth of particles have been treated theoretically and experimentally (Pruppacher and Klett, 1997).

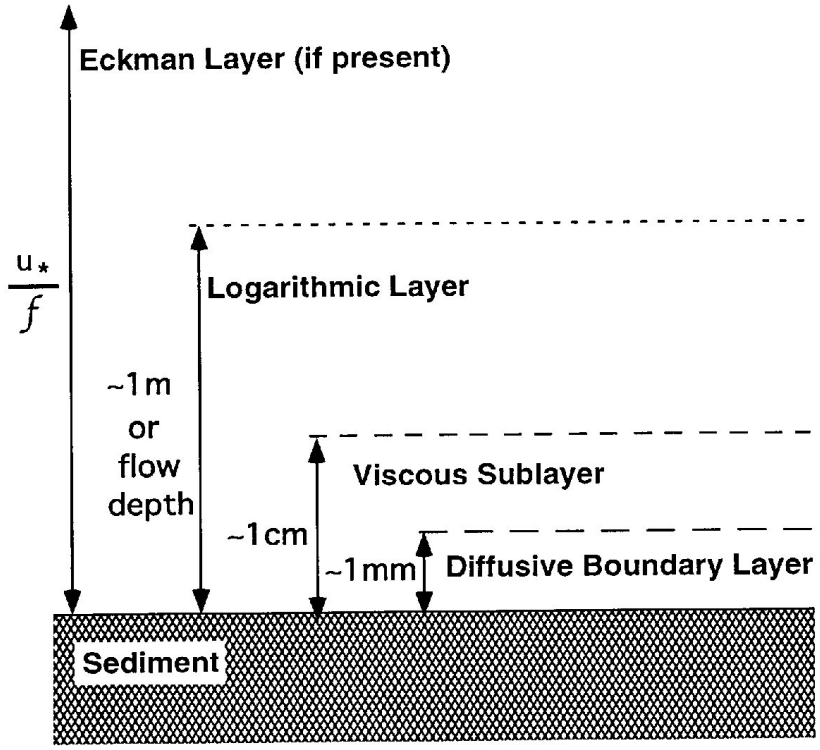


Figure 20: Oceanic boundary layers with approximate scaling laws. From Boudreau and Jørgensen (2001).

# 5 Oceanic bottom boundary layer

One may think of situations where the flux through the bottom is not due to rising $CO_2$ liquid bubbles, either because it is of diffusive nature from a hydrated seafloor, or if the liquid $CO_2$ is denser than seawater. In this case it will be important to model the bottom boundary layer of the ocean. Solute flux depend on the coupling of the interface flux with the turbulence in the boundary layer.

The overall thickness of the oceanic boundary is conventionally defined as the depth where the current has approached the value in the interior of the ocean. Changes within the boundary layer are due to friction in terms of the flow field, but also due to stratification. The frictional boundary layer near the ocean bottom may be characterised by different physical regimes indicated in Figure 20.

## 5.1 Classical scaling laws

A boundary layer drag or friction velocity $U_*$ is conventionally defined as

$$U_*^2 = \frac{\tau}{\rho} = C_w U_\infty^2 \tag{12}$$

where $C_w$ is the quadratic drag coefficient and $U_\infty$ the velocity far away from the interface. Under most oceanic conditions one finds $0.001 < C_w < 0.0025$ and $U_\infty/U_* \approx 20-30$ (Armi and Millard, 1976; Weatherly et al., 1980; Thorpe, 2005). The following thickness estimates assume $U_\infty/U_* = 25$ and illustrate the case $U_\infty = 5$ cm/s ($U_* = 0.2$ cm/s), which is a realistic figure for the deep ocean.

### 5.1.1 Ekman Layer

The largest boundary layer scale is conventionally termed the *Ekman Layer* and often estimated as

$$\delta_E = \frac{\kappa U_*}{f}, \tag{13}$$

where $\kappa \approx 0.4$ is van-Karman's constant and $f$ the Coriolis parameter. With $U_\infty = 5$ cm/s and $f \approx 10^{-4}s^{-1}$ the Ekman Layer is $\delta_E \approx 8$ m.

### 5.1.2 Outer boundary of log-layer

The outer boundary layer or log-layer has its name due to the logarithmic velocity profile given by the *law of the wall*. It is also termed the *constant stress layer*. One has commonly for rough flow

$$U(z) = \frac{U_*}{\kappa} ln \frac{z}{z_0}, \qquad z_0 \approx z_{sedi}/30 \tag{14}$$

where $z$ is the distance from the bottom and $z_{sedi}$ is the roughness of the sediment.

For smooth flow

$$U(z) = \frac{U_*}{\kappa} ln \frac{z}{z_0}, \qquad z_0 \approx 0.1 \frac{\nu}{U_*} \approx \delta_\nu/100 \tag{15}$$

the effective roughness $z_0$ is determined by the viscosity $\nu$ ($\approx 0.016$ cm$^2$/s for deep ocean conditions), or the thickness $\delta_\nu$ of the laminar viscous sublayer, see below. Flow is termed smooth if $z_{sedi} > 3\nu/U_*$. For $U_\infty/U_* = 25$ the log layer has a scale $\delta_{log} \approx e^{10} \times z_0$ or 1.8 meter for smooth flow and $U_* = 0.2$ cm/s.

### 5.1.3 Viscous sublayer

In the viscous sublayer flow is laminar and unaffected by eddies or bottom roughness and the velocity shear is constant. It's scaling

$$\delta_\nu \approx 10 \frac{\nu}{U_*} \tag{16}$$

gives $\delta_\nu \approx 0.8$ cm for smooth flow and $U_* = 0.2$ cm/s.

### 5.1.4 Diffusive sublayer

The fluxes from the bottom are are strongly dependent on the diffusive sublayer commonly scaled as

$$\delta_{diff} \approx \delta_\nu Sc^{-1/3}, \qquad Sc = \nu/D_s(Schmidt \qquad number), \tag{17}$$

where for heat the Schmidt number $Sc$ should be replaced by the Prandtl number. For salt and deep ocean values $\nu/D_s \approx 2.0 \times 10^3$ and $\delta_{diff} \approx 0.6$ mm in case of $U_* = 0.2$ cm/s.

The solute flux in the diffusive sublayer is frequently parametrised in the form

$$F_s \approx D_s \frac{(C_{sat} - C_\infty)}{\delta_{diff}} \approx 0.1 U_* Sc^{-2/3}(C_{sat} - C_\infty). \tag{18}$$

Equation 18 contains the concentration $C_{sat}$ at the interface and $C_\infty$ far away from it where $U_*$ is defined.

## 5.2 Improved models

The boundary layer scales mentioned so far are simplified models that do not consider the complexity of turbulent mixing near the seafloor. The simplest example to illustrate the complexity is to imagine a bottom current driven by its own density. The structure in its boundary layer, and its interaction with the seabed, can be expected to be very different if compared to a boundary layer where a homogeneous or barotropic ocean velocity drops to zero when approaching the sea floor. For proper computation of sea floor solute fluxes it is apparently critical to compute $C_\infty$ and $U_*$ by a turbulence model. Such a model needs to consider several mechanisms that are important near the seafloor, like (i) flow-sediment interaction, (ii) tides, (iii) internal waves, (iv) biological activity.

### 5.2.1 Ekman layer and stratification

Observations show that equation 13 frequently tends to underestimate the bottom boundary layer thickness (Armi and Millard, 1976; Armi, 1978; Weatherly and Martin, 1978). In particular a large variability was found in areas of variable topography (Figure 21). In some cases also a too shallow boundary layer was predicted. Based on dimensional grounds, Weatherly and Martin (1978) proposed the the improved formula

$$\delta_E = A \frac{U_*}{f} \left( \frac{1}{1 + N^2/f^2} \right), \tag{19}$$

where $N^2 = \frac{g}{\rho} \frac{d\rho}{dz}$ represents the stratification and $A \approx 1.3$. For $N \gg f$ the equation passes into $\delta_E = AU_*/(fN)^{1/2}$ derived by Pollard et al. (1973) for deepening wind-mixed layers. Equation 19 accounts both for stratification effects and the generally larger observed $\delta_E$, but it still underestimated the latter in several cases (Weatherly et al., 1980). The latter authors thus agreed with

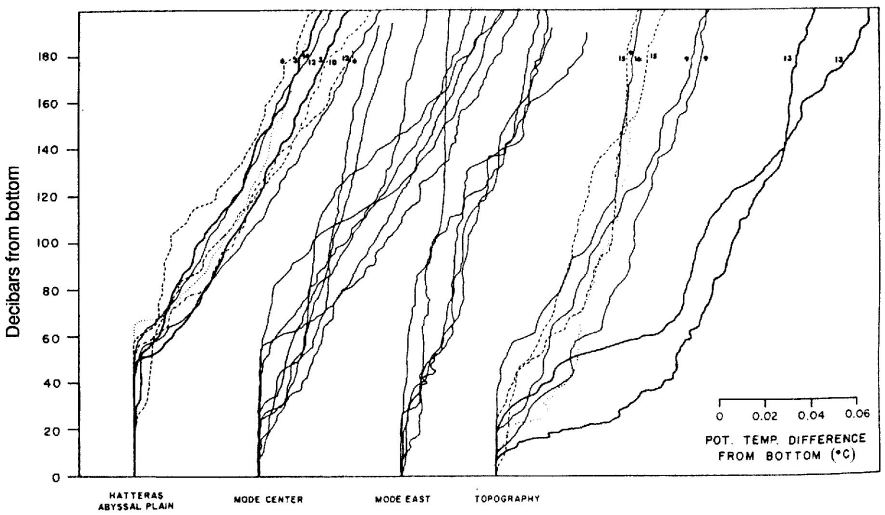


**Figure 8.4.** Profiles of potential temperature over the benthic seabed showing the nature and variability of the near-bottom mixed layer. The vertical axis is height off the bottom. Data are in four groups, moving (left to right) eastward from the flat Hatteras Abyssal Plain onto the rough topography of the mid-Atlantic Ridge where profiles, and mixed layer thickness, are much more variable. The benthic mixed layer is often capped by a sharp change in potential temperature of order 10 mK in 10 m. (From Armi and Millard, 1976.)

Figure 21: Variability in deep sea bottom boundary layers. From Armi and Millard (1976).

Armi (1977) who had pointed out the importance of internal waves as a mixing agent in the deep ocean.

Mixed layer models with more appropriate vertical resolution and turbulence closure schemes have been used in later studies, e.g. (Martin, 1985; Galperin et al., 1988; Kantha and Clayson, 1994; Thorpe, 2005). A semi-empirical treatment of the mixing agency of internal waves was presented by Kantha and Clayson (1994). Diffusion of $CO_2$ from a lake has been simulated both by the standard bulk mixed layer equations given above (Fer and Haugan, 2003) and a more advanced turbulence closure scheme including internal wave parametrisation (Haugan and Alendal, 2005). Some results will be mentioned below.

## 5.3 Ocean-seabed interactions

To find the solute fluxes between the ocean and the seabed the vertical structure in the log-layer close to the sea bottom is particularly important. As an example, Figure 22 from Sanford and Lien (1999) indicates the presence of two log-log-layers close to the bottom, of which one has been attributed by the authors to the presence of form drag, with ripples of the order of 0.3 m height at the sea bottom. An alternative interpretation of this observation has been suggested by Perlin et al. (2005, 2007). The latter authors proposed a simplified approach to calculate the logarithmic velocity profile in the presence of stratification, provided that the mixed layer depth is $\delta_E$ is known.

Any model with emphasis on the solute fluxes near the bottom must focus on

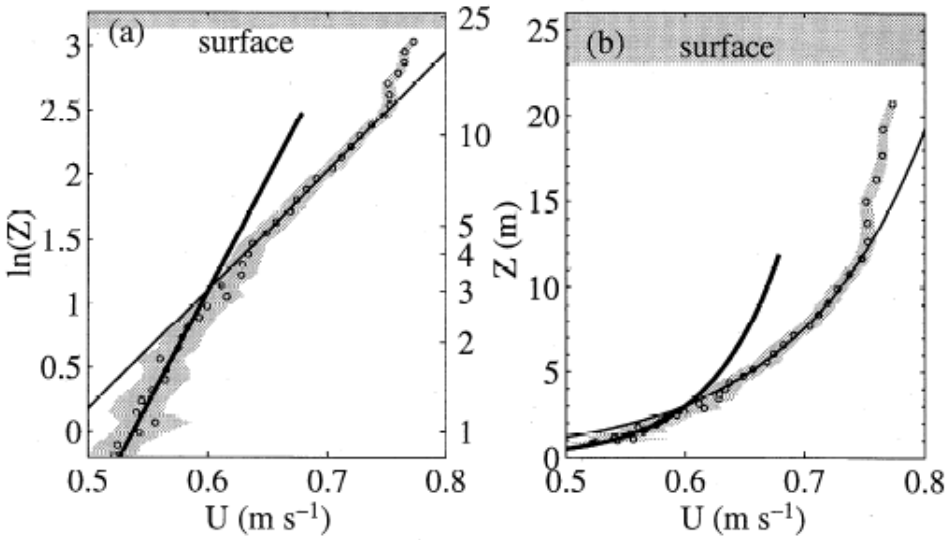


Figure 22: Appearance of two log-layers near the seabed. From Sanford and Lien (1999).

eddy viscosity parameterisations for the particular type of boundary layer. Possible deviations from a log-layer may be related to roughness, interaction with the sediment, the influence of internal waves. Alternative analytical solutions of eddy viscosity schemes have been summarised by Sideman and Pinczewski (1975). Considering the role of suspended sediments, Dade et al. (2001) have compared some model results with the equation 19 from Weatherly and Martin (1978). In Figure 23 the Burger number $S = g\rho' WC/(U_*^2 f)$, where $C$ is sediment concentration and $W$ settling velocity, gives a similar dependence in the reduction of $\delta_E$.

Furthermore may stratification and suspension of sediment in the boundary layer interact in a complex manner with the flow, as shown in Figure 24. It is notable that the settling velocity in this case is computed in a similar way as in section 4 for the rising bubbles.

### 5.3.1 Flux closure and diffusive sublayer $\delta_{diff}$

It is expected that the solute flux from the seafloor not only depends on the parametrisation of the eddy transport close to the interface, yet also on the suspension modes from figure 24. An example of observations of such a diffusive boundary layer is shown in Figure 25. Figure 26 compares two fine-scale boundary layer models in terms of eddy diffusivities. It is seen that, while the models agree on the scale of the viscous boundary layer $\delta_\nu$, they differ on the scale of the diffusive boundary layer. The difference corresponds almost to a factor two in the parametrised interface fluxes, emphasising the problem of boundary layer type.

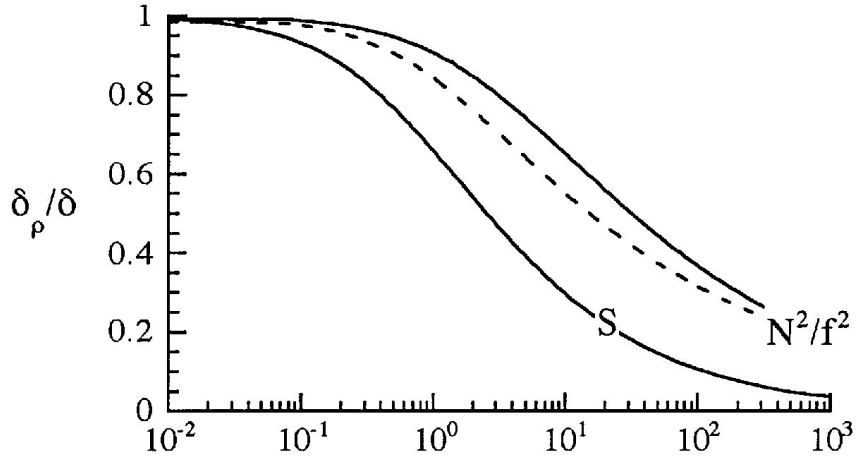


**Figure 2.9** Ratio of thicknesses of stratified and neutral BBLs as functions of $N^2/f^2$ (f = $f$ in figure) and suspended-sediment *Burger number*, S. Dashed line indicates relationship between $\delta_\rho/\delta$ and $N^2/f^2$ proposed by Weatherly and Martin (1978), which was derived under assumptions similar to those made in this analysis.

Figure 23: Decrease in boundary layer depth by suspended sediments. From Dade et al. (2001).

Also from an observational viewpoint there is room for model refinement. The values that have been obtained for the mass transfer velocity, $V_* = c_* U_* Sc^{-2/3}$, often differ from $c_* = 0.10$ approximated in equation 18. Comparing different sources for $Sc = 1000$ the prefactor in equation 18 varies between $c_* = 0.04$ and $c_* = 0.08$, with most values between 0.06 and 0.07 (Boudreau, 2001). It is thus smaller than the frequently assumed value 0.1 Boudreau (2001). Many different schemes and correlations leading to slightly modified parametric dependencies were reviewed by Sideman and Pinczewski (1975). Hence, also the diffusive flux parametrisation at the ocean bottom should be properly validated. The likelihood that a reasonably accurate parameterisation can be found is indicated in Figure 27, which shows the dependence of boundary layer thickness $\delta_{diff}$ on ocean depth. The increase with depth is expected, as one expects slower flow in the deep ocean. The variability is moderate.

In this context also a more detailed look on the fine-scale bottom topography and interaction with the sediment is worth a look. A fine-scale simulation (Figure 28) indicates that bottom irregularities may trigger a convective circulation from as deep as 10 cm within the sediments. The influence of this circulation on matter distribution (figure 28) and diffusive fluxes has been discussed in connection with bio-geochemical processes important on the small scale (Huettel et al., 1998). While obstacles as shown in Figure 28 do not destroy the diffusive sublayer, they have a pronounced effect on the mass transfer. The change of the latter may be expressed in the form

$$\frac{V_{*,rough}}{V_{*,smooth}} = a(\frac{U_* z_b}{\nu})^b Sc^c. \tag{20}$$

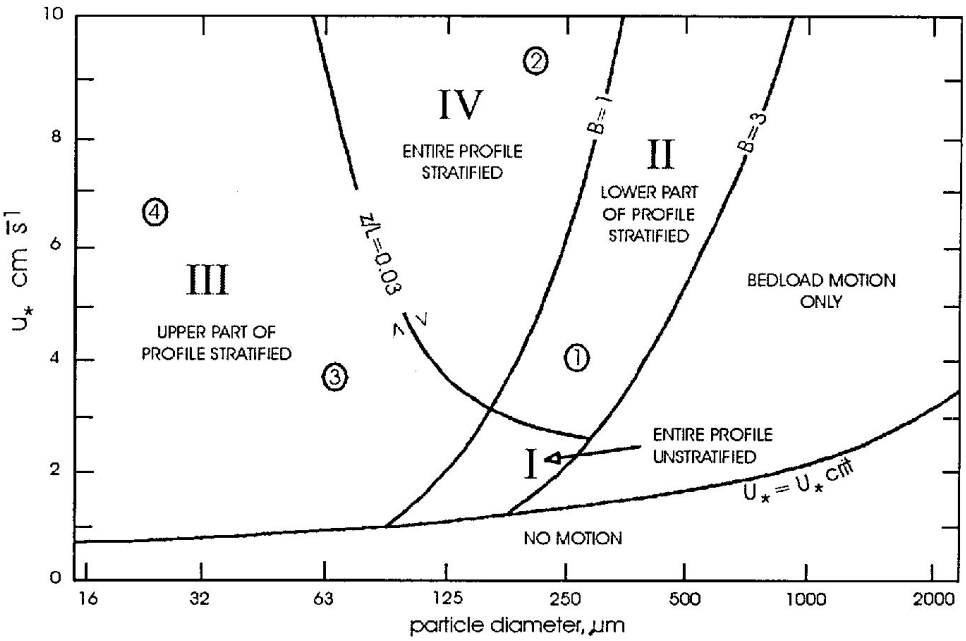


**Figure 4.5** Suspended sediment effect on flow stratification as defined by the stability parameter, $z/L$, and the Rouse Number, $\eta_i = B = w_{si}/\kappa u_*$. Circled numbers indicate the regions in which the velocity profiles shown in figure 4.4 would be found. (From Soulsby and Wainwright, 1987).

Figure 24: Regimes of stratification in dependence on particle size, friction velocity, settling velocity and z/L, where L is the Monin-Obukhov length. From Hill and McCave (2001).

for which a number of studies were compared by Dade et al. (2001). These parameterisations indicate that for $U_* = 0.2$ cm/s the mass transfer from a bottom with roughness 0.1 to 1 cm is likely to be enhanced by a factor of 2 to 4, when compared to a flat surface. Turbulence in flows over rough walls have recently reviewed by Jimenez (2004).

In connection with the convective circulation as deep as 10 cm in sediments (Figure 28) it is of interest that Boudreau (1998) has reported a mean mixed depth of $9.8 \pm 4.5$ cm for sediments. The direct impact of the slow flow on overall diffusive fluxes is likely to be small (if not bio-geo-chemical reactions are considered). However, such an information would be important in understanding the fluxes from the seafloor by consistent modeling of resuspension rates, sublayer stratification and small scale turbulence near the bottom.

### 5.3.2 Internal wave-seabed interaction

While the average mean mixed depth of sediments appears to be $\approx$ 10 cm (Boudreau, 1998), during storm events fluid flow penetration depths of 2-4 meters have been observed (Moore and Wilson, 2005). Comparable magnitudes of seabed instability have been predicted by models of wave-seabed interaction in

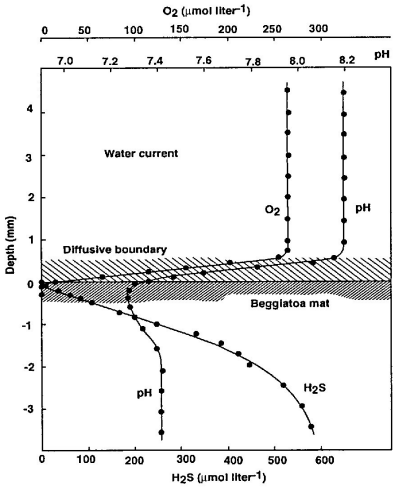


Figure 25: High resolution diffusive boundary layer observations above the seafloor and within the sediments. From Jørgensen (2001).

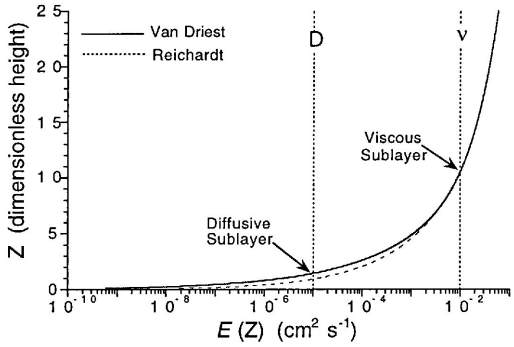


Figure 26: Difference in the diffusive sublayer thickness due to two different model approaches. From Boudreau (2001).

shallow waters (Jeng, 1997). Recently also a theoretical framework of interaction between internal waves and the seabed has been published Chen and Hsu (2005). The latter authors predict that soil displacement on the seabed may reach 40 and 15 m in the horizontal and vertical directions. These scales are similar to the dimension of *pockmarks* on the seafloor (Judd and Hovland, 2007), pointing to the relevance of internal waves in terms of sediment resuspension.

### 5.3.3 Benthic storms

Benthic storms with velocities of $\approx$ 20 cm/s have been reported for different ocean basins, e.g. Polzin et al. (1996); Ledwell et al. (2000); Woodgate and Fahrbach (1999). One might suppose that, in an integral sense, they occur too seldom to influence the slow dissolution from the ocean bottom. However, their role in breaking up a stable stratification could be highly relevant, a process worth of investigation. As extreme events they might shape the seabed and also lead to an effective spreading of leakage over larger distances. The role of benthic storms to eventually breakup the hydrate layer that might form on a $CO_2$ lake in the deep layer was discussed by Fer and Haugan (2003) and Hove and Haugan (2005).

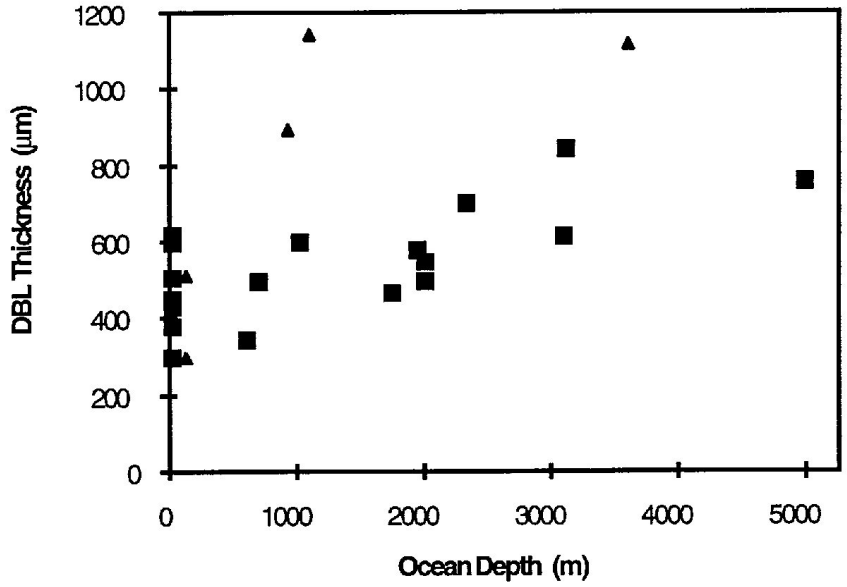


Figure 27: Dependence of diffusive boundary layer thickness on ocean depth. From Jørgensen (2001).

# 6 Mesoscale simulations and observations

## 6.1 Deep sea lake

Fer and Haugan (2003) have performed two-dimensional simulations of dissolution and advection from a 3000 m deep $CO_2$ lake. They performed runs with and without a hydrate layer and reported a 2.7 time higher dissolution rate in the absence of hydrate. However, these results do not appear to be linked to the use of different solubilities in the absence and presence of the hydrate phase, as discussed by Zhang (2005) on the basis of thermodynamic arguments. It appears to be linked to a difference in turbulent closure an flux parametrisation for the two different phases. For example, for the low friction velocity run ($U_\infty = 5$ cm/s), the account of stratification only led to a difference of a factor 1.5. This again points to the need to consider the flux parameterisations near the interface, and their uncertainty, in more detail.

The results obtained by from Fer and Haugan (2003) for the hydrate layer run, based on a solute flux given by equation 18 and a near-bottom velocity of 5 cm/s, are shown in Figure 30. It is seen that the $CO_2$ is confined to a bottom layer of the order of 10 m and spreads over 15 km in the course of three days, which is the expected advection scale. Stratification effects, resulting from the densification of seawater when dissolving $CO_2$, implemented on the basis of equation 19, have also been discussed in this simplified model and are actually included in figure 30. They have the potential to decrease the dissolution rate by a factor of 3 to 5, confining $CO_2$ to a much thinner boundary layer Fer and Haugan (2003).

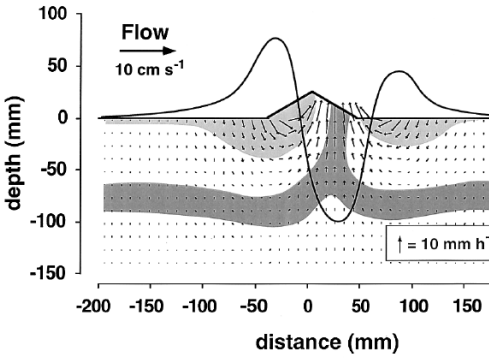


Figure 28: Simulation of flow triggering in the sediment by an obstacle. From Huettel et al. (1998).

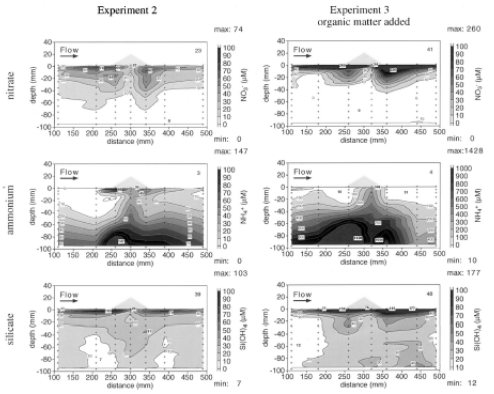


Figure 29: Fine-scale distribution of matter in sediments due to flow. From Huettel et al. (1998).

Similar simulations have been performed with an improved turbulence closure scheme Haugan and Alendal (2005). The latter authors in particular outlined the effect of internal waves which was substantial in increasing the height of the bottom boundary layer, in particular at low velocities. Results are illustrated in Figure 31 for runs without stratification (NIW), including stratification (SIW) and for different velocities $5, 10$ and $20$ cm/s.

The simulations presented so far Fer and Haugan (2003); Haugan and Alendal (2005) are two-dimensional, yet parametrisations are based on validated ocean models that take this idealisation into account. The simulations show the expected influence of stratification on the mixing efficiency of $CO_2$ that dissolves from the ocean bottom and demonstrates that it will be confined to a O(10) m thick bottom boundary layer. Long term simulations are not available. However, based on the generally slow eddy diffusion above the Ekman layer one expects a wide spreading of such a confined signal. For example, a rough estimate of additional layer growth and spread of $CO_2$ by slow eddy diffusion is $\Delta H \approx (K_v L/U_\infty)^{1/2}$ and yields 32 m for L=500 km and $K_v = 10^{-4}$ m$^2$/s.

## 6.2 Droplet plume modelling

Alendal and Drange (2001) simulated the release of droplets of $CO_2$ from a source at oceanic mid depth, where $CO_2$ is lighter than seawater. While the bubbles are rising they dissolve and make the ambient water more dense, which then starts sinking. The principal behaviour of such a system is to some degree resembled by Figure 24. There is a critical diameter above which droplets continue rising and below which they are simply advected by the mean flow. In the simulations by Alendal and Drange (2001) this diameter was 0.5 mm. The vertical extension of the evolving plume thus increases with increasing initial droplet size. For droplets of the order of $1 - 2$ cm diameter it was found to be typically 30-50 m, when evaluated some 100 m from the source.

Simulations by Alendal and Drange (2001) assumed (i) liquid, (ii) noninteracting bubbles (iii) without a hydrate skin. In reality (i) underestimates

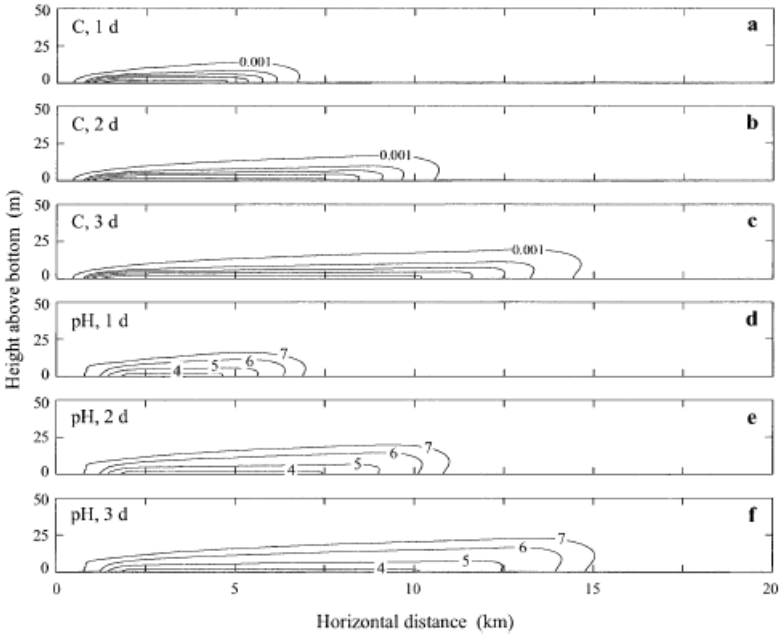


Figure 30: Simulations of height and advection of $CO_2$ (and pH changes) dissolving from a hydrate-covered lake over the course of 3 days. From Fer and Haugan (2003).

the spreading because the terminal velocity should be based on solid particles (although, as discussed in section 4, irregular droplet shapes would in turn increase the drag). The neglect of interaction (ii) also overestimates the rise velocity. Furthermore, the use of $CO_2$ solubility should be corrected for the presence of hydrate (Zhang, 2005), which would decrease dissolution and thus increase the height to which bubbles rise. The results from Alendal and Drange (2001) also indicate the behaviour of droplet plumes, when released from the bottom of shallower seas. In such a scenario concentration of $CO_2$ will also be restricted to a shallow regime close to the source. In shallow seas, however, mixing by winds is much more relevant and the mixing can be expected to be more efficient on length-scales of hundreds of kilometers. Then, of course, $CO_2$ returns to the atmosphere.

Recent observations of rise velocities (Chen et al., 2003) indicate that also in the presence of a hydrate shell droplets are elliptical, with increasing drag and a terminal velocity plateau as seen in Figure 19. The droplets in the experiment discussed by Chen et al. (2003) were, however, strongly interacting. To what degree the simulations by Chen et al. (2003) are realistic therefore depends essentially on the the above mentioned question of droplet geometry and interaction. The effective parameterisations that they used were similar to those employed by Alendal and Drange (2001). The results were also comparable, with the difference that the Chen et al. (2003) performed simulations for a bottom release: The main density increase was confined to a layer of a few

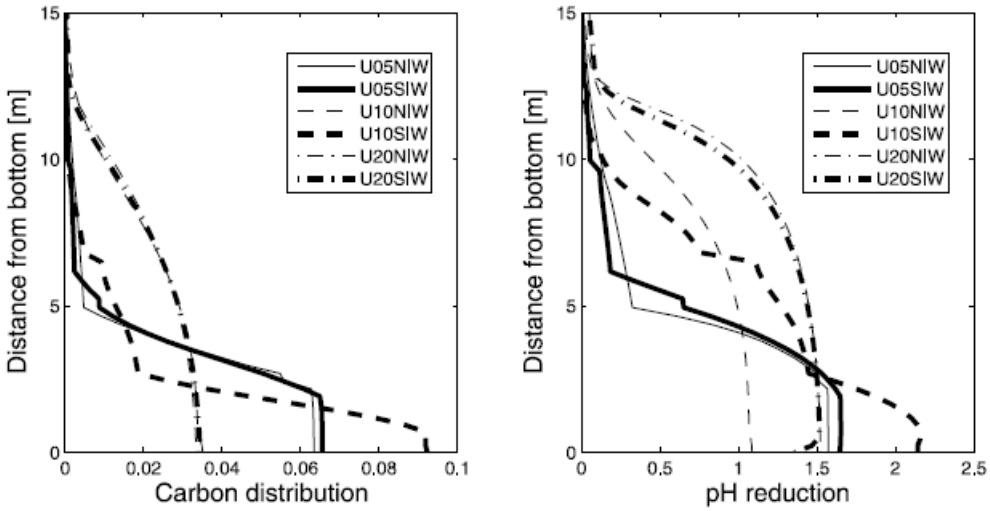


Figure 31: Simulations of distribution of $CO_2$ and pH reduction in the bottom boundary layer 7500m from the source after 3 days. From Haugan and Alendal (2005).

tenths of meter above the bottom, and the thickness of this layer increased with initial droplet diameter. Chen et al. (2005) have further compared simulations for droplet release at mid depth.

Recently, Brewer et al. (2006) reported similar simulations, treating the rising velocity on the basis of the liquid drop drag coefficient parameterisations from Chen et al. (2005). Their application is in so far inconsistent, that they use a drag parametrisation for a liquid droplet, while arguing that the observed bubbles are assumed perfectly spherical, which they propose due to the rigid hydrate shell.

Clearly, more accurate evaluations of shape and interaction effects on the drag are needed. On the one hand, this may be done in sensitivity studies of numerical simulations (Alendal and Drange, 2001; Chen et al., 2003, 2005). On the other hand, it is likely that the sensitivity on droplet behaviour may be obtained by simplified boundary layer models. An useful goal of future studies could be to establish bounds and parameter regimes like in Figure 24 for interaction of bottom sediment buoyancy with the mean flow.

### 6.3 Observations

There are no observations available that might validate the modelling of dissolution from the sea bottom on the large scale (as investigated by Fer and Haugan (2003) and Haugan and Alendal (2005)). The small-scale experiments performed so far with small containers (Brewer et al., 2004; Hove and Haugan, 2005) not even allow the detection of a signal more than 1 m away from these samples. Here the progress essentially depends on model studies.

Observations of single droplets tracked by an ROV (Brewer et al., 2002),

already discussed above, might also suffer from the influence of the ROV on the droplet movement. Recently, experiments on the release of cloud of droplets have been reported. These were monitored by acoustic means and could be tracked by some 150 m (Brewer et al., 2006). Such observations seem to be promising to analyse the rising behaviour of interacting droplets. However, the volumes of $CO_2$ that may be realised under such experiments appear too small to create the critical increase in the ambient water density that results in the double-plume formation as discussed by Alendal and Drange (2001) and Chen et al. (2003).

Indirect validations of models may be performed by studying natural seep areas of gas bubbles (Judd and Hovland, 2007). For example, an interesting area is located in the Western Barents Sea where large methane plumes are observed in a pockmark field (Lammers et al., 1995). The latter is insofar of interest as horizontal currents and tidal excursions are relatively well known, and due to seasonal variability in the stability characteristics of the bottom boundary in this area.

## 6.4 Longterm perspectives and climate model simulations

In the long term the $CO_2$ from the discussed potential source will spread with ocean currents. Its return to the atmosphere will depend on the evolution of $CO_2$ content therein, and the bio-geo-chemical carbon cycle. A global simplified model study has been performed by Khesgi and Archer (2004). Studies with climate and global circulation models, that more thoroughly treat the release and source functions of $CO_2$, focusing on the longterm changes and distribution of near-bottom pH, do not exist yet.

# 7 Fluxes through the seabed

The present report closes with a remark on physical processes related to the long term safety on geological sub-sea-storage, illustrated by Figure 32. Many studies support that longterm climate changes were influenced by catastrophic release of the strong greenhouse gas methane (Kvenvolden, 1993; Wefer et al., 1994; Dickens et al., 1995; Nisbet, 2002; Zhang, 2003). One may therefore speculate that changes in the ocean bottom temperature, as they are expected under the global warming scenarios, have the potential to change certain seabed regimes, in terms of their permeability and trapping behaviour, if methane hydrate is liquefied by warming. Taking the propagation of an oceanic warming signal into the seabed as $Z \approx 2(\kappa t)^{1/2}$, and using $\kappa \approx 10^{-6}$ m$^2$/s for the heat diffusivity, one may obtain an estimate of 80-200 years for the propagation through the typical hydrate stability zone of thickness 100-200 m. The response is slow, but operates on the timescale of climate change (and its mitigation). Moreover may gas hydrate destabilisation be triggered by other more rapid mechanisms related to structural changes in the seabed, e.g., Suess et al. (1999).

Another important question is to what degree the seabed stability may be modified when $CO_2$ dissolves in the water of the formation where it is to be stored. The following process chain may be imagined. 1.) Dissolution implies an overall increase in the density. 2.) The density increase leads to convection in the formation (this has been simulated, see IPCC (2007b)). 3.) Convection then brings saturated brine to levels of higher temperature, making the solution over-saturated. It needs to be considered to what degree these diffuso-convective processes can lead to heterogeneity in the pore structure and might trigger fracturing.

## 7.1 Permeability and Percolation

In any case it is important to consider the possible change in seabed permeability that either climate change or storage of a reactive compound as $CO_2$ may trigger, and be aware of the timescales. An important aspect of catastrophic permeability changes may be illustrated as follows. Flow through porous media at low Reynolds number is normally described by the classical seepage velocity $V$ law after Darcy

$$V = \frac{K}{\mu}\frac{dP}{dz}, \tag{21}$$

with dynamic viscosity $\mu$ and pressure gradient $dP/dz$. The permeability $K$ is a measure of the characteristic cross-sectional area of pores normal to flow. It depends on tortuosity, connectivity and porosity $\phi$. Empirically $K \sim \phi^m$ with a most frequent range $2 < m < 5$ is found. Theoretically $m = 2$ and 3 for arrays of cylinders and slots where the connectivity is not changing. A constant $m \approx 3$ is also frequently assumed in reservoir modelling.

However, in natural porous media forming by some kind of random compaction the permeability is often controlled by a network of the largest pores. Such a system may be described by percolation theory (Shante and Kirkpatrick, 1971; Thompson et al., 1987; Stauffer, 1991; Sahimi, 1993; Hunt, 2005b,a) which

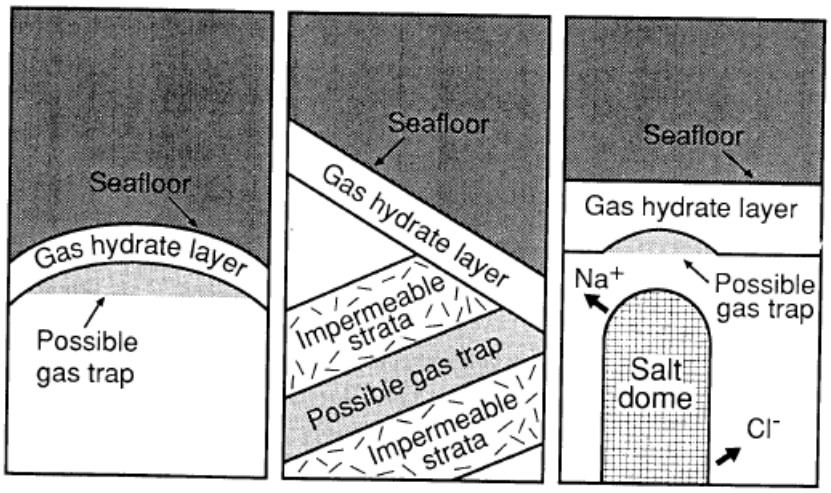


**Figure 10.** Schematic diagrams of geological situations in which gas hydrates serve as seals forming traps for methane. Developed from *Dillon et al.* [1980].

Figure 32: Trapping of gas and liquids due to sealing in the gas hydrate stability regime. From Kvenvolden (1993).

yields an effective $K'$ via an equation of the form

$$\frac{K'}{K} =\sim (\phi - \phi_c)^q, \tag{22}$$

where $\phi_c$ is the critical porosity at which the connectivity vanishes. Theoretically one finds that$\phi_c \approx 0.29$ and $q \approx 1.9$ for the three-dimensional isotropic continuum. For anisotropic inclusions and systems of pores $\phi_c$ can be considerably smaller. Its value for most three-dimensional lattices where the bonds are closed by a random process is $\approx 0.15$ (Shante and Kirkpatrick, 1971; Sahimi, 1993).

Natural systems often operate near thresholds. In porous media the critical behaviour near the threshold is often related to a certain porosity [2]. Then a very small change in the porosity may lead to extreme changes in the permeability. This is illustrated in Figures 33 and 34 and has been observed in many other materials. The threshold may, however, have rather different values, depending on the connectivity of different pores. The example near the base of the stability illustrated in Figure 14 has, for example, an overall porosity of 0.5, but the percolation apparently takes place through the largest pores that occupy $\approx 0.2 \times 0.5 = 0.1$. A small change in the heterogenity and pore distribution of this material, driven by either natural climate change, or $CO_2$-related chemical

[2]Threshold behaviour may also be related to the onset of chemical reactions upon reaching a certain thermodynamic state (Shante and Kirkpatrick, 1971; Stauffer, 1991)

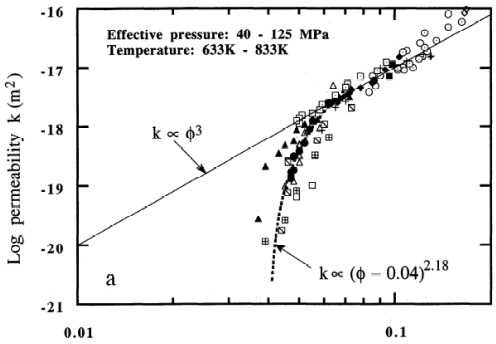


Figure 33: Permeability of hot-pressed calcite, showing a sharp deviation from $K \sim \phi^3$ above the percolation threshold of $\phi_c \approx 0.04$. From Zhang et al. (1994).

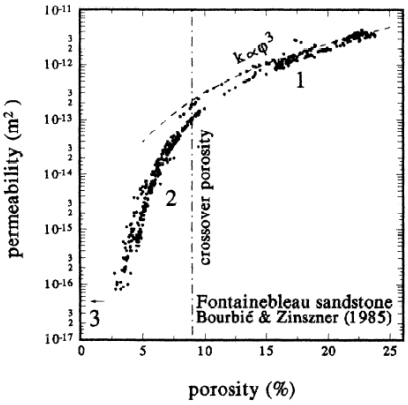


Figure 34: Permeability of sandstone with an increasing deviation from $K \sim \phi^3$ near a crossover porosity of $\approx 0.08$. From Zhu et al. (1995).

processes within the formation, might shift the system to a state above the percolation threshold.

Percolation theory allows the evaluation of the critical macroscopic behaviour of large systems on the basis of microscopic observations and localised chemo-physical state transitions. Its importance to interpret geological systems has recently been outlined (Sahimi, 1993; Selyakov and Kadet, 1996; Berkowitz and Ewing, 1998; Hunt, 2005b). Future reservoir modelling has a clear perspective in this field of research. Percolation thresholds and nonlinear network permeability of seabeds appear as an important topic in order to properly evaluate of longterm safety of geological carbon storage.

# 8 Summary and outlook

It is recalled from the introductory section 1, that Carbon Capture and Storage (CCS) (i) requires a considerably larger overall energy production, and that (ii) its role to mitigate climate change is limited to a bridging period of 100 to 200 years. Within this time frame a fully renewable energy infrastructure needs to be established, if serious socio-economical and ecological problems for humans on earth are to be avoided.

The goal of the present report was to provide an overview about the physical processes that need to be understood to evaluate risks of $CO_2$ leakage through the sea floor, as a possible consequence of geological sub-sea storage during this bridging period. The main conclusions of the present limited report are summarised as follows:

- Section 2. Thermodynamics and phase equilibria of $CO_2$-seawater mixtures and of $CO_2$-hydrate are well established for the oceanic PVTx-regime. There is, however, future need for proper extension of thermodynamic models and state equations to high pressure regimes that are required for accurate reservoir modelling.

- Section 3. Microstructural details of porous media are important to properly model seepage through the seabed, in particular when considering metastability and phase transitions in the hydrate-stability regime. The yet unsolved problem of a hydrate shell around a $CO_2$ droplet rising through seawater might be adressed in a multidisciplinary way, for example by including structural information from hydrates forming from the ice phase, in a much more easily accessible PT-regime.

- Section 4. Most applications to date have not properly distinguished between drag and dissolution of liquid and rigid $CO_2$-droplets rising through seawater. The influence of droplet shape, interaction and coagulation, and the details of local convective boundary layers also need to be properly established. This also points to the importance of properly understanding hydrate shell thermodynamics and morphology (section 3).

- Section 5. Modifications of classical boundary layer models in terms of sediment suspension, stratification and internal waves are known to be important to understand bottom boundary layer mixing in the ocean. To understand $CO_2$ fluxes from the seafloor also viscous and diffusive sublayer models need to be critically reviewed. The topic of internal wave seabed interactions has received little interest yet. It is of particular importance in situations of strongly stratified $CO_2$-saturated bottom layers.

- Section 6. Long-term large-scale simulations of $CO_2$-leakage by global models are lacking. To validate mesoscale simulations very large amounts of $CO_2$ would be required in release experiments. It appears to be most realistic to look for information on ion fluxes from the sea floor, as available in the field of geochemistry and deep sea biology. Considering droplet

plume dynamics, the field of cloud physics stands as an established empirical-theoretical framework, from which much can be learned to constrain modelling approaches.

- Section 7. Investigations of catastrophic fluxes through the seafloor should be extended by modern theories of percolation and probability. This is a challenge for future reservoir modelling.

## References


Adams, J., Bachu, S., 2002. Equations of state for geofluids: algorithm review and intercomparison of brines. Geofluids 2, 257–271.

Alendal, G., Drange, H., 2001. Two-phase, near-field modeling of purposefully released $CO_2$ in the ocean. J Geophys. Res. 106 (C1), 1085–1096.

Alendal, G., Haugan, P. M., Gangstø, R., Caldeira, K., Adams, E., Brewer, P., Peltzer, E., Rehder, G., Sato, T., Chen, B., 2006. Comment on 'fate of rising $CO_2$ droplets in seawater. Envir. Sci. Technolog. 40 (11), 3653–3654.

Anderson, R., Llamedo, M., Tohidi, B., Burgass, R. W., 2003a. Characteristic of clathrate hydrate equilibria in mesopores and interpretation of experimental data. J. Phys. Chem. B 107, 3500–3506.

Anderson, R., Llamedo, M., Tohidi, B., Burgass, R. W., 2003b. Experimental measurement of methane and carbon dioxide clathrate hydrate equilibria in mesoporous silica. J. Phys. Chem. B 107, 3507–3514.

Archer, D., 2005. Fate of fossil fuel $CO_2$ in geological time. J. Geophys. Res 110, C09S05.

Archer, D. G., 1992. Thermodynamic properties of the NaCl + $H_2O$ system: II. thermodynamic properties of NaCl(aq) and $NaClH_2O$(cr), and phase equilibria. J. Phys. Chem. Ref. Data 21 (4), 793–829.

Armi, L., 1977. The dynamics of the bottom boudary layer of the deep ocean. Elsevier Scientific, pp. 153–164.

Armi, L., 1978. Some evidence for boundary mixing in the deep ocean. J. Geophys. Res. 83 (C4), 1971–1979.

Armi, L., Millard, R. C., 1976. The bottom boundary layer of the deep ocean. J Geophys. Res. 81, 4983–4990.

Aya, I., Yamane, K., Nariai, H., 1997. Solubility of $CO_2$ and density of $CO_2$ hydrate at 30 MPa. Energy 22 (2/3), 263–271.

Batchelor, G. K., 1967. An introduction to fluid mechanics. Cambridge University Press, 615 pp.

Berkowitz, B., Ewing, R., 1998. Percolation theory and network modeling - applicationsin soil physics. Surv. Geophys. 19, 23–72.

Bhaga, D., Weber, M. E., 1981. Bubbles in viscous liquids: shapes, wakes and velocities. J. Fluid Mech. 105, 61–85.

Boudreau, B. P., 1998. Mean mixed sediments: the wherefore and the why. Limnolog. Oceanogr. 43 (3), 524–526.

Boudreau, B. P., 2001. Solute transport above the sediment-water interface. In: Boudreau, B. P., Jørgensen, B. B. (Eds.), The benthic boundary layer. Oxford University Press, Ch. 5.

Boudreau, B. P., Jørgensen, B. B., 2001. The benthic boundary layer. Oxford University Press.

Bozzano, G., Dente, M., 2001. Shape and terminal rise velocity of single bubble motion. Comp. Chemic. Engin. 25, 571–576.

Bradshaw, A., 1973. The effect of carbon dioxide on the specific volume of seawater. Limnol. Oceanogr. 18 (1), 95–105.

Brewer, P. G., Chen, B., Warzinki, R., Baggeroer, A., Peltzer, E., Dunk, R. M., Walz, P., 2006. Three-dimensional acoustic monitoring and modeling of a deep-sea $CO_2$ droplet cloud. Geophys. Res. Letts. 33, L23607S.

Brewer, P. G., Peltzer, E., Aya, I., Haugan, P., Bellerby, R., Yamane, K., Kojima, R., Walz, P., Nakajima, Y., 2004. Small scale field study of an ocean $CO_2$ plume. J. Oceanogr. 60, 751–758.

Brewer, P. G., Peltzer, E. T., Friederich, G., Orr, F. M., 1999. Direct experiments on the ocean disposal of fossil fuel $CO_2$. Science 284, 943–945.

Brewer, P. G., Peltzer, E. T., Friederich, G., Rehder, G., 2002. Experimental determination of the fate of rising $CO_2$ droplets in seawater. Environ. Sci. Technol. 36, 5441–5446.

Buffett, B. A., 2000. Clathrate hydrates. Annu. Rev. Earth Planet. Sci. 28, 477–507.

Caldeira, K., Wickett, M. E., 2003. Oceanography: anthropogenic carbon and ocean ph. Nature 425, 365.

Chandrasekhar, S., 1961. Hydrodynamic and Hydromagnetic Stability. Clarendon Press, 652 pp.

Chen, B., Song, Y., Nishio, M., Akai, M., 2003. Large-eddy simulation of double-plume formation induced by $CO_2$ dissolution in the ocean. Tellus 55B (2), 723–730.

Chen, B., Song, Y., Nishio, M., Someya, S., Akai, M., 2005. Modeling near-field dispersion from direct injection of carbon dioxide into the ocean. J. Geophys. Res. 110, C09S15.

Chen, C. Y., Hsu, J. R. C., 2005. Interaction between internal waves and a permeable seabed. Ocean Engineering 32, 587–621.

Clark, J. F., Washburn, L., Harnafius, J. S., Luyendyk, B. P., 2000. Dissolved hydrocarbon flux from natural marine seeps to the southern California Bight. J. Geophys. Res. 105 (C5), 11509–11522.

Clennell, M. B., Hovland, M., Booth, J. S., Henry, P., Winters, W. J., 1999. Formation of natural gas hydrates in marine sediments 1. Conceptual model of gas hydrate growth conditioned by host sediment properties. J. Geophys. Res. 104 (B10), 22985–23003.

Clift, R., Grace, J. R., Weber, M. E., 1978. Bubbles, drops and particles. Academic Press, 380 pp.

Dade, W. B., Hogg, A. J., Boudreau, B. P., 2001. Physics of flow above the sediment-water interface. Oxford University Press, Ch. 2.

Davies, R. M., Taylor, G., 1950. The mechanics of large bubbles rising through extended liquids and through liquids in tubes. Proc. Roy. Soc. Lond. A 200 (1062), 375–390.

Demurov, A., Radhakrishnan, R., Trout, B. L., 2002. Computations of diffusivities in ice and $CO_2$ clathrate hydrates via molecular dynamics and Monte Carlo simulations. J. Chem. Phys. 116 (2), 702–710.

Dickens, G. R., O'Neil, J. R., Rea, D. K., Owen, R. M., 1995. Dissociation of oceanic methane hydrate as a cause of the carbon isotope excursion at the end of the paleocene. Paleooceanogr. 10 (6), 965–971.

Duan, Z., Sun, R., 2003. An improved model calculatiingf $co_2$ solubility in pure water and aqueous nacl solutions from 273 to 533 K and from 0 to 2000 bar. Chem. Geolog. 193, 257–271.

Duan, Z., Sun, R., 2006. A model to predict phase equilibrium of $CH_4$ and $CO_2$ clathrate hydrate in aqueous electrolyte solutions. Amer. Mineral. 91 (8-9), 1346–1354.

Duan, Z., Sun, R., Zhu, C., Chou, I. M., 2006. An improved model for the calculation of $CO_2$ solubility in aqueous solutions containing $Na^+$, $K^+$, $Ca^+$, $Mg^{2+}$, $Cl^-$, and ${SO_4}^{2-}$. Marine Chemistr. 98, 131–139.

Ely, J. F., Haynes, W. M., Bain, B. C., 1989. Isochoric (p, vm, t) measurents on $CO_2$ and on ($0.982CO_2$ + 0.018 $N_2$) from 250 to 330 k at pressures to 35 mpa. J. Chemic. Thermodyn. 21 (8), 879–894.

Feistel, R., 2003. A new extended Gibbs thermodynamic potential of seawater. Progr. in Oceanogr. 58, 43–114.

Fer, I., Haugan, P. M., 2003. Dissolution from a liquid film. Limnol. Oceanogr. 48, 872–883.

Fischedick, M., Esken, A., Luhmann, J. J., Schuewer, D., Supersberger, N., 2007. Geologische $CO_2$-Speicherung als klimapolitische Handlungsoption. Wuppertal spezial 36, Wuppertaler Institut f. Klima, Umwelt, Energie.

Fofonoff, P., Millard, R. C., 1983. Algorithms for computation of fundamental properties of seawater. Unesco Tech. Pap. in Mar. Sci. 44, 53 pp.

Frank, X., Funfschilling, D., Midoux, N., Li, H. Z., 2006. Bubbles in a viscous liquid: lattice Boltzmann simulation and experimental validation. J. Fluid Mech. 546, 113–122.

Gabitto, J., Tsouris, C., 2006. Dissolution mechanisms of $CO_2$ hydrate droplets in deep seawaters. Energy Convers. Mgmt. 47, 494–508.

Gale, J., 2004. Geological storage of $CO_2$: What do we know , where are the gaps and what more needs to be done? Energy 29, 1329–1338.

Galperin, B., Kantha, L. H., Hassid, S., Rosati, A., 1988. A quasi-equilibrium turbulent energy model for geophysical flows. J. Atmospher. Sc. 45, 55–62.

Gangstø, R., Haugan, P. M., Alendal, G., 2005. Parameterization of drag and dissolution of rising $CO_2$ drops in seawater. Geophys. Res. Letters 32, L10612.

Gebhart, B., Jaluria, Y., Mahajan, R., Sammakia, B., 1988. Buoyancy-induced Flows and Transport. Hemisphere Publishing.

Genov, G., Kuhs, W. F., Staykova, D., Goreshnik, E., Salamantin, A. N., 2004. Experimental studies on the formation of porous gas hydrates. Amer. Mineralogist 89, 1228–1239.

Gershuni, G. Z., Zhukovitskii, E., 1976. Convective stability of incompressible fluids. Israel Program for Scientific Translations, Keter Publishing House, in russian 1972 by Izdatel'stvo Nauka, Jerusalem, 329 pp.

Göttlicher, G., 2006. Entwicklungsmöglichkeiten der $CO_2$-Rühaltung in Kraftwerken aus thermodynamischer Sicht. Chem. Ing. Techn. 78 (4), 407–415.

Handa, Y. P., 1990. Effect of hydrostatic pressure and salinity on the stability of gas hydrates. J. Phys. Chem. 94, 2652–2657.

Happel, J., Brenner, J., 1986. Low Reynolds Number Hydrodynamics. M. Nijhoff, Dordrecht, Netherlands, 553 pp.

Harper, J. F., 1972. The motion of bubbles and drops through liquids. Adv. Appl. Mech. 12, 59–129.

Haugan, P. M., Alendal, G., 2005. Turbulent diffusion and transport from a $CO_2$ lake in the deep ocean. J. Geophys. Res. 110 (S), C09S14.

Henry, P., Thomas, M., Clennell, M. B., 1999. Formation of natural gas hydrates in marine sediments 2. Thermodynamic calculations of stability conditions in porous sediments. J. Geophys. Res. 104 (B10), 23005–23022.

Hill, P. S., McCave, I. N., 2001. Suspended particle transport in benthic boundary layers. In: Boudreau, B. P., Jørgensen, B. B. (Eds.), The benthic boundary layer. Oxford University Press, Ch. 4.

Hillig, W. B., 1998. Measurement of interfacial free energy for the ice/water system. J. Cryst. Growth 183, 463–468.

Hobbs, P., 1974. Ice Physics. Clarendon Press, Oxford, 837 pp.

Holder, G. D., Cugini, A. V., Warzinski, R. P., 1995. Modeling clathrate hydrate formation during carbon dioxide injection into the ocean. Environ. Sci. Technolog. 29, 276–278.

Hove, J., Haugan, P. M., 2005. Dynamics of a $CO_2$-seawater interface in the deep ocean. J. Mar. Res. 63, 563–577.

Hu, J., Duan, Z., Zhu, C., Chou, I. M., 2005. PVTx properties of the $CO_2$-$H_2O$ and $CO_2$-$H_2O$-NaCl systems below 647 K: Assessment of experimental data and thermodynamic models. Chemic. Geolog. 238, 249–267.

Hua, J., Lou, J., 2007. Numerical simulation of a bubble rising in viscous fluid. J. Computat. Phys. 222, 769–795.

Huettel, M., Ziebis, W., forster, S., Luther, G. W., 1998. Advective transport affecting metal and nutrient distributions and interfacial fluxes in permeable sediments. Geochimica and Cosmochimica Acta 62 (4), 613–631.

Hunt, A., 2005a. Basic transport properties in natural porous media. Complexity 10 (3), 22–37.

Hunt, A., 2005b. Percolation theory for flow in porous media. Lecture notes in physics. Springer, 203 pp.

IAPWS, 2003. Revised release on the IAPS formulation 1985 for the viscosity of ordinary water substance. Tech. rep., International Association for the Properties of Water and Steam, Vejle, Denmark.

Inamuro, T., Ogata, T., Tajuma, S., Konishi, N., 2004. A lattice Boltzmann method for incompressible two-phase flows with large density differences. J. Comput. Physics 198, 628–644.

IPCC, 2007a. Climate change 2007: The physical science basis. Tech. rep., Intergovernmental Panel on Climate Change.

IPCC, 2007b. IPCC Special Report: Carbon dioxide capture and storage. Tech. rep., Intergovernmental Panel on Climate Change.

Ishikiriyama, K., Todoki, M., Motomura, K., 1995. Pore size distribution (psd) measurements of silica gels by means of scanning differential scanning calorimetry. I. Optimization for determination of psd. J. Colloid Interf. Sci. 171, 92–102.

Jeng, D. S., 1997. Wave-induced seabed instability in front of a breakwater. 1997 24 (10), 887–917.

Jimenez, J., 2004. Turbulent flows over rough walls. Annu. Rev. Fluid. Mech. 36 (36), 173–196.

Johnston, O., Santillo, D., Stringer, R., Partentier, R., Hare, B., Krueger, M., March 1999. Ocean disposal/sequestration of carbon dioxide from fossil fuel production and use: an overview of rationale, techniques and implications. Tech. rep., Greenpeace Research Lab.

Jørgensen, B. B., 2001. Physics of flow above the sediment-water interface. In: Boudreau, B. P., Jørgensen, B. B. (Eds.), The benthic boundary layer. Oxford University Press, Ch. 14.

Joseph, D., 2003. Rise velocity of a spherical cap bubble. J. Fluid Mech. 488, 213–223.

Judd, A. G., Hovland, M., 2007. Seabed Fluid Flow. Cambridge University Press.

Kalbaliyev, G., Ceylan, K., 2007. Development of new emperical equations for estimation of drag coefficient, shape deformation, and rising velocity of gas bubbles or liquid drops. Chem. Eng. Comm. 194, 1623–1637.

Kang, I. S., Leal, L. G., 1988. The drag coefficient for a spherical bubble in a uniform streaming flow. Phys. Fluids 31 (2), 233–237.

Kantha, L. H., Clayson, C. A., 1994. An improved mixed layer model for geophysical applications. J. Geophys. Res. 99 (C12), 25235–25266.

Katsuki, D., Ohmura, R., Ebinuma, T., Narita, H., 2007. Methane hydrate crystal growth in a porous medium filled with methane saturated liquid water. Phil. Mag. 87 (7), 1057–1069.

Kerr, R. C., 1994. Dissolving driven by vigorous compositional convection. J. Fluid Mech. 280, 287–302.

Kerr, R. C., 1995. Convective crystal dissolution. Contrib. Mineral. Petrol. 121, 237–246.

Khesgi, H., Archer, D. E., 2004. A nonlinear convolution model for the evasion of CO2 injected into the deep ocean. J. Geophys. Res. 109, doi:10.1029/2002JC001489.

Klapproth, A., Goreshnik, E., Staykova, D., Klein, H., Kuhs, W. F., 2003. Structural studies of gas hydrates. Canad. J. Phys. 81, 503–518.

Krishna, R., Urseanu, M. I., Baten, J. M., Ellenberger, J., 1999. Rise velocity of a swarm of gas bubbles in liquids. Chemic. Eng. Sci. 54, 171–183.

Kuhs, W. F., Genov, G., Goreshnik, E., Zeller, A., Techmer, K., 2004. The impact of porous microstructures of gas hydrates on their macroscopic properties. Int. J. Offshore and Polar Engin. 14 (4), 305–309.

Kuhs, W. F., Klapproth, A., Gotthardt, F., Techmer, K., 2000. The formation of meso- and macroporous gas hydrates. Geophys. Res. Lett. 27 (18), 2929–2932.

Kvenvolden, K. A., 1993. Gas hydrates - geological perspective and global change. Rev. Geophys. 31 (2), 173–187.

Lammers, S., Suess, E., Hovland, M., 1995. A large methane plume east of Bear Island (Barents Sea): implications for the marine methane cycle. Geol. Rundsch. 84, 59–66.

Ledwell, J. R., Montgomery, E. T., Polzin, K. L., Schmitt, R. W., Toole, J. M., 2000. Evidence for enhanced mixing over rough topography in the abyssal ocean. Nature 403, 179–182.

Lerman, A., 1979. Geochemical processes water and sediment environments. Wiley and Sons, 481 pp.

Levich, V. G., 1962. Physicochemical hydrodynamics. Prentice-Hall, Englewood Cliffs (first Russian edition 1952), 699 pp.

MacCracken, M. C., 2006. Geoengineering: worthy of cautious evaluation? Clim. Change 77, 235–243.

Marchetti, C., 1977. On geoengineering and the $CO_2$ problem. Clim. Change 1, 59–68.

Martin, P. J., 1985. Simulation of the mixed layer at OWS November and Papa with several models. J. Geophys. Res. 90, 903–916.

Maxworthy, T., Gnann, C., Kuerten, M., Durst, F., 1996. Experiments on the rise of air bubbles in clean viscous fluids. J. Fluid Mech. 321, 421–441.

Miller, S. L., 1961. The occurrence of gas hydrates in the solar system. Proc. Nat. Acad, Sci. of the U.S.A. 47 (11), 1798–1808.

Moore, D. W., 1959. The rise of gas bubble in a viscous fluid. J. Fluid Mech. 6, 113–130.

Moore, D. W., 1963. The boundary layer on a spherical bubble. J. Fluid Mech. 16, 161–176.

Moore, W., Wilson, A. M., 2005. Advective flow through the upper continental shelf driven by storms, buoyancy, and submarine groundwater discharge. Earth Plant. Sci. Lt. 235, 564–576.

Mori, Y., 1998. Clathrate hydrate formation at the interface between liquid $CO_2$ and water phases - a review of rival models characterizing 'hydrate films'. Energy Convers. 39 (15), 1537–1557.

Mori, Y. H., Mochizuki, T., 1997. Mass transport across clathrate hydrate films - a caplillary permeation model. Chem. Eng. Sci. 52, 3613–3616.

Mori, Y. H., Murakami, T., 2007. Can the thickness of hydrate films on $CO_2$ drops be estimated from the buoyant motion? A critique of a previous paper. Energy Convers. Mgmt. 48 (48), 494–499.

Nealson, K., 2006. Lakes of liquid $CO_2$ in the deep sea. PNAS 103 (38), 13903–13904.

Nisbet, E., 2002. Have sudden large releases of methane from geological reservoirs occurred since the last galcial maximum, and could such releases occur again? Phil. Trans. R. Soc. Lond. A 360, 581–607.

Ogasawara, K., Yamasaki, A., teng, H., 2001. Mass transfer from $CO_2$ drops traveling in high-pressure and low-temperature water. Energy Fuels 15, 147–150.

Ohmura, R., Shimada, W., Uchida, T., Mori, Y., Takeya, S., Nagao, J., Minegawa, H., Ebinuma, T., Narita, H., 2004. Clathrate hydrate crystal growth in liquid water saturated with a hydrate-forming substance: variations in crystal morphology. Phil. Mag. 84 (1), 1–16.

Østergård, K. L., Anderson, R., Llamedo, M., Tohidi, B., 2002. Hydrate phase equilibria in porous media: effect of pore size. Terra Nova 14 (5), 307–312.

Parson, E. A., Keith, D. W., 1998. Fossil fuels without $CO_2$ emissions. Science 282, 1053–1054.

Perlin, A., Moum, J. N., Klymak, J. M., Levine, M. D., Boyd, T., Kosro, P. M., 2005. A modified law-of-the-wall applied to oceanic bottom boundary layers. J. Geophys. Res. 110, C10S10.

Perlin, A., Moum, J. N., Klymak, J. M., Levine, M. D., Boyd, T., Kosro, P. M., 2007. Organization of stratification, turbulence, and veering in bottom Ekman layers. J. Geophys. Res. 112, C05S90.

Pitzer, K. S., Peiper, J. C., Bussy, R. H., 1984. Thermodynamic properties of aqueous sodium chloride solutions. J. Phys. Chem. Ref. Data 13 (1), 1–102.

Pitzer, K. S., Sterner, S. M., 1995. Equations of state valid continously from zero to extreme pressures with $H_2O$ and $CO_2$ examples. Int. J. Thermosphs. 16 (2), 511–518.

Pollard, R. T., Rhines, R. B., Thompson, R. O. R., 1973. The deepening of the wind-mixed layer. Geophys. Fluid Dyn. 3, 381–404.

Polzin, K. L., Speer, K. G., Toole, J. M., Schmidt, R. W., 1996. Intense mixing of Antartic bottom water in the equatorial Atlantic Ocean. Nature 380, 54–57.

Pruppacher, H. R., Klett, J. D., 1997. Microphysics of clouds and precipitation, 2nd Edition. Vol. 18 of Atmospheric and oceanographic sciences library. Kluwer Acadamics Publ., 954 pp.

Radhakrishnan, R., Demurov, A., Herzog, H., Trout, B. L., 2003. A consistent and verifiable macroscopic model for the dissolution of liquid $CO_2$ in water under hydrate forming conditions. Energy Conversion and Management 44, 771–780.

Raupach, M., Marland, G., Ciais, P., Le Quere, C., Canadell, J. G., Klepper, G., Field, C. B., 2007. Global and regional drivers of accelerating $CO_2$ emissions. PNAS 104 (24), 10288–10299.

Sahimi, M., 1993. Flow phenomena in rocks. Rev. of Mod. Phys. 65 (4), 1393–1534.

Sanford, T. B., Lien, R. C., 1999. Turbulent properties in a homogeneous tidal bottom boundary layer. J. Geophys. Res. 104 (C1), 1245–1257.

Schlichting, H., 2004. Boundary Layer Theory, 8th Edition. Springer, 801 pp.

Selman, J. R., Tobias, C. W., 1978. Mass-transfer measurements by the limiting-current technique. Adv. Chem. Engineer. 10, 211–318.

Selyakov, V. I., Kadet, V. V., 1996. Percolation models for transport in porous media - with applications to reservoir engineering. Vol. 9 of Theories and applications of transport in porous media. Kluwer Academic, 241 pp.

Shante, J. F., Kirkpatrick, S., 1971. An introduction to percolation theory. Adv. Phys. 20 (85), 325–357.

Sideman, S., Pinczewski, W. V., 1975. Turbulent heat and mass transfer at interfaces: transport models and mechanisms. In: Gutfinger, C. (Ed.), Topics in transport phenomena. Hemispher Publishing, Ch. 2.

Sloan, E. D., 1998. Clathrate hydrates of natural gases. Marcel Dekker.

Sloan, E. D., 2004. Introductory review. Amer. Minerlogist 89, 1155–1161.

Song, Y., Chen, B., Nishio, M., Akai, M., 2005. The study of density change of carbon dioxide seawater solution at high pressure and low temperature. Energy 30, 2298–2307.

Stauffer, D., 1991. Introduction to Percolation Theory, 2nd Edition. Taylor & Francis.

Stavins, R., 1999. The costs of carbon sequestration. Americ. Econ. Rev. 89 (4), 994–1009.

Staykova, D., Kuhs, W. F., Salamantin, A. N., Hansen, T., 2003. Formation of porous gas hydrates from ice powders: diffraction experiments and multistage model. J. Phys. Chem. B 107, 10299–10311.

Stern, L., Cicerone, S., Kirby, S., June 2005. SEM imaging of gas hydrate formation pocesses and growth textures, and comparison to natural hydrates of marine and permafrost origin. Proceedings 5th Int. Conf. on Gas Hydrates, Trondheim, Norway.

Stern, L. A., Kirby, S., Circone, S., Durham, W. B., 2004. Scanning electron microscopy investigations of laboratory-grown gas clthartes hydrates formed from melting ice, and comparison to natural hydrates. Amer. Mineralogist 89, 1162–1175.

Suess, E., Torres, M. E., Bohrmann, G., Collier, R. W., Greinert, J., Linke, P., Rehder, G., Trehu, A., Wallman, K., Winckler, G., Zuleger, E., 1999. Gas hydrate destabilization: enhanced dewatering, benthic material turnover and large methane plumes at the Cascadia convergent margin. Earth and Planetary Science Letters 170, 1–15.

Sugaya, M., Mori, Y., 1996. Behaviour of a clathrate hydrate formation at the boundary of liquid water and a fluorocarbon in liquid and vapor state. Chem. Engin. Sci. 51 (13), 3505–3517.

Sun, R., Duan, Z., 2007. An accurate model to predict the thermodynamic stability of methane hydrate and methane solubility in marine environments. Chem. Geolog. 244, 248–262.

Svandal, A., Kvamme, B., Granasy, L., Pusztai, T., Buanes, T., Hove, J., 2006. The phase-field theory applied to $CO_2$ and $CH_4$ hydrate. J. Cryst. Growth 287, 468–490.

Tewes, F., Boury, F., 2004. Thermodynamic and dynamic properties of binary carbon-dioxide-water systems. J. Phys. Chem. B 108, 2405–2412.

Thomas, D. G., Armistead, R. A., 1968. Concentration-gradient-driven convection: Experiments. Science 160 (3831), 995–996.

Thompson, A. H., Katz, A. J., Krohn, C. E., 1987. The microgeometry and transport properties of sedimentary rock. Adv. in Physics 36, 625–694.

Thorpe, S. A., 2005. The turbulent ocean. Cambridge university press, 439 pp.

Tiller, W. A., 1991. The science of crystallization: macroscopic phenomena and defect generation. Cambridge University Press, 484 pp.

Turner, J. S., 1973. Buoyancy Effects in Fluids. Cambridge University Press, 367 pp.

Uchida, T., Ebinuma, T., Takeya, S., Nagao, J., Narita, H., 2002. Effects of pore sizes on dissociation temperatures and pressures of methane, carbon dioxide, and propane hydrates in porous media. J. Phys. Chem. B 106, 820–826.

Udachin, K. A., Ratcliffe, C. I., Ripmeester, J. A., 2001. Structure, composition and thermal expansion of $CO_2$ hydrate from single crystal x-ray diffraction measurements. J Phys. Chem. B 105, 4200–4204.

v. Stackelberg, M., 1949. Feste Gashydrate. Naturwissenschaften 36 (12), 327–333, 359–362.

Weatherly, G., Martin, P. J., 1978. On the structure and dynamics of the oceanic boundary layer. J. Phys. Oceanogr. 8, 557–570.

Weatherly, G. L., Blumsack, S. L., Bird, A. A., 1980. On the effect of diurnal tidal currents in determing the thickness of the turbulent ekman boundary layer. J. Phys. Oceanogr. 10, 297–300.

Wefer, G., Heinye, P. M., Berger, W. H., 1994. Clues to ancient methane release. Nature 369, 282.

Woodgate, R., Fahrbach, E., 1999. Benthic storms in the greenland sea. Deep-Sea Res. I 46, 2109–2127.

Xu, T., Apps, J. A., Pruess, K., 2003. Reactive geochemical transport simulation to study mineral trapping for $CO_2$ disposal in deep areanceous formations. J. Geophys. Res. 108 (B2), 2071.

Xu, W., 2004. Modeling dynamic marine gas hydrate systems. Amer. Mineralog. 89, 1271–1279.

Yamane, K. I., Aya, I., Namie, S., Narai, H., 2000. Strength of CO2 hydrate membrane in seawater at 40 mpa. Ann. N.Y. Acad. Sci. 912, 254–260.

Zatsepina, O. Y., Buffett, B. A., 2001. Experimental study of the stability of $CO_2$-hydrate in a porous medium. Fluid Phase Equil. 192, 85–102.

Zatsepina, O. Y., Buffett, B. A., 2003. Nucleation of gas hydrate in marine environments. Geophys. Res. Lett. 30, 1451.

Zaytsev, I. D., Aseyev, G. G., 1992. Properties of aqueous solutions of electrolytes. CRC Press, Boca Raton, 1773 pp.

Zhang, J., Fan, L. S., 2003. On the rise velocity of an interactive bubble in liquids. Chemic. Engin. J. 92, 169–176.

Zhang, S., Paterson, M. S., Cox, S. F., 1994. Porosity and permeability evolution during hot isostatic pressing of calcite aggregates. J. Geophys. Res. 99 (B8), 15741–15760.

Zhang, Y., 2003. Methane escape from gas hydrate systems in marine environment, and methane-driven oceanic eruptions. Geophys. Res. Let. 30, 1398.

Zhang, Y., 2005. Fate of rising $CO_2$ droplets in seawater. Environ. Sci. Technol. 39, 7719–7724.

Zhang, Y., Xu, Z., 2003. Kinetics of convective crystal dissolution and melting, with applications to methane hydrate dissolution and dissociation in seawater. Earth Planet. Sci. Let. 213, 133–148.

Zhu, W., David, C., Wong, T., 1995. Network modeling of permeability evolution during cementation and hot isostattic pressing. J. Geophys. Res. 100 (B8), 15451–15464.